UC Riverside

UC Riverside Electronic Theses and Dissertations

Title

Does Selective Breeding for High Voluntary Wheel-Running Behavior Alter the Pelvis in a Sex-Specific Manner?

Permalink

https://escholarship.org/uc/item/0hk3n1rn

ISBN

9798173720016

Author

Ibarra Zea, Marisol

Publication Date

2026-08-24

Supplemental Material

https://escholarship.org/uc/item/0hk3n1rn#supplemental

Peer reviewed|Thesis/dissertation

eScholarship.org Powered by the California Digital Library
University of California

UNIVERSITY OF CALIFORNIA
RIVERSIDE

Does Selective Breeding for High Voluntary Wheel-Running Behavior Alter the Pelvis in a Sex-Specific Manner?

A Thesis submitted in partial satisfaction
of the requirements for the degree of

Master of Science

in

Evolution, Ecology, and Organismal Biology

by

Marisol B. Ibarra Zea

September 2026

Thesis Committee:

- Dr. Theodore Garland, Jr., Chairperson
- Dr. Natalie Holt
- Dr. Crystal Reynaga

Copyright by
Marisol B. Ibarra Zea
2026

The Thesis of Marisol B. Ibarra Zea is approved:

Committee Chairperson

University of California, Riverside

ACKNOWLEDGEMENTS

Academic Acknowledgments

I am deeply grateful to my Principal Investigator, Dr. Theodore Garland, Jr., for his unwavering support since the very beginning of my time in his lab. I also extend my thanks to all present and past Garland Lab members whose collective efforts made this multigenerational project possible. Separately, many thanks to our UK collaborators, Dr. Katrina Jones and Elisabeth Webb, for their partnership and alignment with our work.

I would like to thank my committee members, Dr. Natalie Holt and Dr. Crystal Reynaga, for their invaluable feedback. Dr. Holt went above and beyond throughout my journey in the program, generously giving time to help me develop as a scientist. Dr. Reynaga has been a wonderful source of inspiration, and I have learned so much from her background and experiences.

Dr. Wendy Saltzman is the reason my decision to choose UCR was an easy yes. Despite having just met me at the time, she offered continuous support and encouragement during my application process. Because of her genuine interest in my success, regardless of where I ultimately chose to go, joining the EEOB department to do my master's at UCR felt like an unquestionable choice.

Dr. Ernesto Vargas-Parra always made himself available for any questions as I navigated the 3DGM world and graduate school, which was entirely new to me. I learned firsthand the importance of being supportive of others and encouraging, and I thank him for making my learning curve with different softwares much less intimidating.

Supported by NSF grant IOS-2038528, a Butterfly Project Fellowship, and a P.O.D.E.R Scholarship.

Personal Acknowledgments

Thank you to all of my loved ones who provided positivity and support when I needed it most. It truly takes a village.

My siblings were my initial motivation to pursue a path I genuinely enjoy. Coming from a background filled with limitations and obstacles, the desire to be a steady, reliable presence in their lives has always pushed me to keep going. Thank you for being my anchor. I hope this adds to our shared journey of knowing que sí se puede; es difícil, pero se puede.

Most importantly, my fur children have been an endless source of happiness and daily motivation. Through long hours spent at the computer working, they proved to be the ultimate coworkers anyone could ever wish for. I am eternally grateful for their presence in my life, as I truly would not be the person I am today without them. No milestone would feel complete or worth celebrating without them by my side.

ABSTRACT OF THESIS

Does Selective Breeding for High Voluntary Wheel-Running Behavior Alter the Pelvis in a Sex-Specific Manner?

by

Marisol B. Ibarra Zea

Master of Science, Evolution, Ecology, and Organismal Biology
University of California, Riverside, September 2026
Dr. Theodore Garland, Jr., Chairperson

The pelvis is the attachment site for vertebrate hindlimbs and is responsible for supporting the weight of the upper body and transferring it to the lower limbs, facilitating balance and mobility. The pelvis is composed of the sacrum, coccyx, and paired hip bones (ilium, ischium, pubis). Research comparing species with different locomotor behaviors indicates that pelvic morphology in terrestrial mammals may be shaped, in part, by evolutionary trade-offs between reproductive demands and locomotor performance. We used the artificially selected High Runner (HR) lines of mice to analyze pelvic morphology in relation to daily movement distance and sex. In this model, outbred house mice (*Mus domesticus*; Hsd:ICR strain) were bred for increased voluntary wheel-running behavior to create four HR lines and four non-selected Control (C) lines. These lines have been used to study correlated responses in exercise physiology, behavior, neurobiology, and genetics. Whole-body CT images were

obtained from 190 mice at generation 93. Pelvic size and shape were analyzed with 3D geometric morphometrics, based on 44 landmarks.

We expected divergence in pelvic morphology between the HR and C lines, and that this would be greater for males than for females because the latter are somewhat constrained by reproductive demands. We also tested for differences among the replicate HR lines to examine the possibility of multiple solutions.

With body length as a covariate, HR lines did not significantly differ from C lines in pelvic centroid size, but the pelvis was larger in females than males, with no linetype-by-sex interaction. In contrast, pelvic shape (with or without body size or centroid size as a covariate), was affected by both linetype and sex, but with no linetype-by-sex interaction, therefore not supporting our differential constraint hypothesis.

At the level of variation among replicate lines, pelvic shape was more dispersed in morphospace in HR lines as compared with C lines, for both sexes. This result suggests "many-to-one mapping" as a mechanism that has led to "multiple solutions" in response to a uniform selective regime imposed on the four replicate HR lines.

TABLE OF CONTENTS

1. Introduction 1
1.1. Pelvis in general 1
1.2. Pelvis in Relation to Locomotion in Quadrupeds 1
1.3. Sexual Dimorphism (and Sexual Selection) 6
1.4. Study System 8
1.6. Hypotheses 10
2. Methods 12
2.1. Organismal Model and Selection Regime 12
2.2. Specimens 13
2.3. Three-Dimensional μCT Analysis and Reconstruction 14
2.4. Statistical Analysis of Body Size and Pelvis Centroid Size 14
2.5. Pelvis Isolation, Landmark Collection, Visualization, and Statistical Analyses 15
3. Results 18
3.1. Body Length 18
3.2. Pelvis Centroid Size 19
3.3. Pelvis Shape 20
Pelvis Shape for Both Sexes 20
Shape by Line 21
Shape by Females 22
Shape by Males 23
Shape by Female HR Lines 24
Shape by Female C Lines 25
Shape by Male HR Lines 25
Shape by Male C Lines 26
4. Discussion 28
Overall Findings in Relation to Hypotheses 28
Multiple Solutions and Many-to-One Mapping 30
Modular Adaptation: Birth vs. Locomotion 32

Obstetric Module and Sexual Dimorphism 32
Locomotor Adaptations and the Cursorial Hypothesis 33
Caveats, Limitations, and Future Directions 34
Methodological Refinements and Linear Measurements 34
Sampling and Phenotypic Plasticity 36
Integrative Analyses of Skeletal Evolution 37
Acknowledgments 37
References Cited in Zotero 81
Supplemental Files 88

LIST OF FIGURES

Figure 1 Whole-Body Scan of Same Mouse (ID 96186) 65

Figure 2 44 Landmarks in Methods (ID 96186) 67

Figure 3 A) Body Length & B) Centroid Size 2 Panels by Line and Sex from SAS 69

Figure 4 A) PC1 vs PC2 Both Sexes; B) X, Y TPS Grid PC1 and PC2 71

Figure 5 A) PC4 vs PC4 Both Sexes; B) X, Y TPS Grid PC3 and PC4 …….....74

Figure 6 PC1 vs PC2 by Line Females and Then Males 77

Figure 7 PC3 vs PC4 by Line Females and Then Males 79

Figure 8 Morphological Disparity (all 125 PCAs) 81

LIST OF TABLES

Table 1 – Sample Size for Control and High Runner Mice 39

Table 2 – Body Length and Centroid Size from SAS 40

Table 2A Body Length by Sex and Linetype 40

Table 2B Body Length by Linetype for Females 42

Table 2C Body Length by Linetype for Males 43

Table 2D Centroid Size with Body Length as a Covariate by Sex and Linetype 44

Table 2E Centroid Size with Body Length as a Covariate by Linetype for Females 46

Table 2F Centroid Size with Body Length as a Covariate by Linetype for Females 47

Table 3 — Shape ANOVA All Mice (No Covariate, with Length, with Centroid) 48

Table 3A Pelvis Shape for Both Sexes (1N) 48

Table 3B Pelvis Shape for Both Sexes with Length (1L) 49

Table 3C Pelvis Shape for Both Sexes with Centroid Size (1S) 49

Table 4 — Shape ANOVA All Mice by LINE Both Sexes (No Covariate, Length, Centroid) 50

Table 4A (4N)--HR No Covariate 50

Table 4B (5N) --C No Covariate 51

Table 4C (4L) --HR Length 51

Table 4D (5L) --C Length 51

Table 4E (4S) -- HR Centroid 52

Table 4F (5S)--C Centroid 52

Table 5— Shape ANOVA FEMALE No Covariate, with Length, with Centroid 53

Table 5A (2N) — Shape ANOVA FEMALE No Covariate ….....53

Table 5B (2L)— Shape ANOVA FEMALE with LENGTH 53

Table 5C (2S)— Shape ANOVA FEMALE with CENTROID SIZE 54

Table 6— Shape ANOVA MALE (No covariate, with Length, with Centroid) 55

Table 6A (3N) — Shape ANOVA MALE No Covariate 55

Table 6B (3L)— Shape ANOVA MALE with LENGTH as Covariate 55

Table 6C (3S)— Shape ANOVA MALE with CENTROID SIZE as Covariate 56

Table 7— Shape ANOVA FEMALE HR LINES (No Covariate, with Length, with Centroid) 57

Table 7A (6N) — Shape ANOVA Female HR Lines No Covariate 57

Table 7B (6L)— Shape ANOVA Female HR Lines Length 57

Table 7C (6S)— Shape ANOVA Female HR Lines Centroid Size 58

Table 8— Shape ANOVA FEMALE C LINES (no covariate, with length, with Centroid) 59

Table 8A (8N) — Shape ANOVA Female C Lines No Covariate 59

Table 8B (8L) — Shape ANOVA Female C Lines Length 59

Table 8C (8S) — Shape ANOVA Female C Lines Centroid Size 60

Table 9— Shape ANOVA MALE HR LINES (No Covariate, with Length, with Centroid) 61

Table 9A (7N) — Shape ANOVA Male HR Lines No Covariate 61

Table 9B (7L) — Shape ANOVA Male HR Lines length 61

Table 9C (7S)— Shape ANOVA Male HR Lines Centroid Size 62

Table 10— Shape ANOVA Male C Lines (No Covariate, with Length, with Centroid) 63

Table 10A (9N)— Shape ANOVA Male C Lines No Covariate 63

Table 10B (9L) — Shape ANOVA Male C Lines Length 63

Table 10C (9S)— Shape ANOVA Male C Lines Centroid Size 64

1. Introduction

1.1. Pelvis in general

The **pelvis** (sacrum, coccyx, and paired hip bones [os coxae; composed of the ilium, ischium, and pubis]) serves as a critical functional interface, responsible for the transmission of propulsive forces from the hindlimbs to the torso and the distribution of axial body weight to the appendicular skeleton (Dalstra and Huiskes 1995; Lewton et al. 2020). Selection on locomotor behavior is expected to engender **correlated, adaptive changes** in pelvic structure that enhance force transmission, stability, and energetic efficiency. Accordingly, the mammalian pelvis has received considerable study.

1.2. Pelvis in Relation to Locomotion in Quadrupeds

Numerous studies have examined pelvic characteristics in relation to locomotion in quadrupeds, especially how the pelvis is related to cursoriality. Before considering some examples, it is important to note that the definition of "cursoriality" is complicated. In a review of the literature, Carrano (1999) noted multiple definitional aspects, including: 1) an animal that can run, run often or for

long distances; 2) has parasagittal oriented limbs; 3) larger animals specialized as a result of limb scaling at large body sizes; 4) morphology-based differences; 5) performance-based differences; 6) mechanical relevance for locomotion. Thus, studies can vary widely in how they define cursoriality, including Kelly et al. (2006) and (Garland, Jr. and Janis 1993).

In a broad-based comparative study of 123 species, Álvarez et al. (2013) found that in saltatorial and bipedal species, such as kangaroo rats (*Dipodomys* sp.) and spring hare (*Pedetes capensis*), the pelvis has an elongated ilium and ischio-pubic complex. Cursorial species, including the cheetah (*Acinonyx jubatus*), gray wolf (*Canis lupus*), and Patagonian mara (*Dolichotis patagonum*), have an elongated ilium and a wide vertical ramus of the ischium. Conversely, ambulatory mammals like the hog-nosed skunk (*Conepatus chinga*) and crab-eating raccoon (*Procyon cancrivorus*) typically have an open acetabulum and a relatively short ischio-pubic complex. Finally, trotter species, such as the Western European hedgehog (*Erinaceus europaeus*) and the wombat (*Vombatus ursinus*), are characterized by an extremely reduced symphysis and ischium body (Álvarez et al. 2013).

In a study of 46 species of modern Carnivora and 27 extinct ones, Martín-Serra et al. (2014) concluded that body size (allometry) and phylogeny appear to be the primary drivers of hind limb morphology (femur, tibia, and pelvis taken

together), with locomotor behavior playing a secondary role. Even so, examining these structures across different taxa reveals clear functional contrasts in skeletal robustness. For instance, cursorial canids have slender hind limbs that may facilitate energetic efficiency, whereas distantly related ursids (e.g., the extinct cave bear and giant panda), the semifossorial European badger, and extinct saber-toothed cats (*Smilodon* and *Barbourofelis*), have robust bone morphologies that could be more suited to withstanding the mechanical stresses of capturing large prey. In addition, Martín-Serra et al. (2014) concluded that allometric shape changes (with pelvises exhibiting larger areas in larger-bodied species) may provide increased attachment space for proximal limb muscles. Ultimately, the authors suggest that the appendicular skeleton in mammalian carnivores is an example of "one-to-many" pattern of evolution between phenotype and function (Martín-Serra et al. 2014).

In a more recent study of 33 species of Carnivora, Lewton et al. (2020) found results that corroborated those of Martin-Serra (2014) in showing that phylogeny and body size have greater effects on the three-dimensional (3D) shape of the carnivoran pelvis than does locomotor behavior, which they categorized into six locomotor "groups" (arboreal, cursorial, natatorial, scansorial, semifossorial, terrestrial). Nevertheless, examining pelvic morphology across these specific locomotor groups reveals some anatomical patterns. For instance, many terrestrial species (e.g., felids) have square-shaped pubic bones with long

symphyses, whereas other terrestrial groups (e.g., herpestids [mongooses]) have narrower ilia and more slender ischia. In addition, scansorial taxa, such as ursids, have the widest and most laterally flaring iliac blades in the sample, though the authors note this is likely driven by positive allometric changes related to body size rather than climbing demands. Similarly, cursorial canids are characterized by longer ilia and shorter ischia, whereas semifossorial skunks have a triangular pelvis with long pubic rami and short symphyses. In contrast, the arboreal locomotor type seen in species such as palm civets is associated with a pelvis featuring wide ilia and broad ischia.

In contrast, research on 12 species of Felidae by Pallandre et al. (2021) indicates that pelvic morphology, specifically the inter-iliac angle, is more related to locomotor behavior (e.g., climbing, pack hunting) than to phylogeny and allometry. Cursorial specialists, such as the cheetah, have a long and narrow pelvis, with a highly acute angle, which is thought to enhance joint stiffness to resist pitching moments during high-speed gallops. Arboreal species have wider pelvic angles, hypothesized to support the leg abduction required for climbing. In contrast, scansorial and terrestrial felids have intermediate angles.

In a study of 30 species of echimyid rodents and eight species of octodontoid, Tavares and Pessôa (2020) found that, after correcting for variation in body size, epigean species, such as the terrestrial spiny rats (*Proechimys*

simonsi and *Thrichomys inermis*), have an elongated pelvis, with a quadrangular shape and a long distance between the acetabulum and femoral tubercle, which is suggested to provide the power and stability needed for rapid terrestrial acceleration. Arboreal taxa, including the bamboo rat (*Kannabateomys amblyonyx*) and the painted tree rat (*Callistomys pictus*), have a short distance between the femoral tubercle and acetabulum and a large femoral head with a short greater trochanter, possibly helping with extreme hip mobility and load-bearing capacity required for climbing. In contrast, fossorial rodents (e.g., *Carterodon sulcidens* and *Clyomys laticeps*) have a short, wide pubic body and a broad obturator foramen resulting in a triangular ischiopubic region, which likely increases the area for hip adductor muscles used to stabilize the body while digging. Finally, semi-aquatic species such as the coypu (*Myocastor coypus*) are characterized by a posteriorly elongated pubic body and a high ischial tuberosity located close to the acetabulum, which is suggested to promote the strong propulsive force needed for the swimming power stroke (Tavares and Pessôa 2020).

Despite numerous studies (Csanády et al. 2019; Mpagike and Makungu 2024; Belyaev et al. 2025). However, the selective factors that have led to the adaptive evolution of pelvis size and shape are not fully understood, nor are the potential constraints and functional trade-offs that may be involved (Lewton 2015; Esteban et al. 2020).

1.3. Sexual Dimorphism (and Sexual Selection)

Differential functional requirements, such as those related to weight bearing, parturition, locomotion, and attachment of muscles can lead to the evolution of sexual size dimorphism (Csanády et al. 2019). Aside from functional demands related to locomotion, the mammalian pelvis is also uniquely shaped by the physical and physiological requirements of reproduction. As these requirements typically differ between the sexes, one might expect some degree of sexual dimorphism in the pelvis. Indeed, the pelvis is sexually dimorphic in many species, including laboratory rodents, with females generally having larger and wider pelvic apertures that facilitate the passage of neonates (McPherson and Chenoweth 2012).

In the genus *Urocyon*, two species of foxes (*U. cinereoargenteus* and *U. littoralis*) exhibit significant sexual dimorphism in pelvic shape. However, only *U. littoralis* had sexual dimorphism in pelvis size, and *U. cinereoargenteus* did not have dimorphic size (Schutz et al. 2009b). Specifically, males in both species typically have a larger acetabulum and a wider, longer obturator foramen. In contrast, females feature a longer, wider iliopubic ramus and a shorter pubic symphysis to accommodate a larger birth canal. The authors suggest that the pelvic dimorphism is driven by a functional constraint of efficient cursorial

locomotion (which favors a narrow pelvis) and the reproductive necessity of giving birth to proportionately large offspring (which requires a broad pelvis).

In a comparative study of two species, larger quadrupedal mammals, such as wolves and Eurasian lynx, males have larger pelvic bones than females, with the most significant differences found in the breadth of the ilium and size of the acetabulum (Csanády et al. 2019). Female wolves had a slightly wider pelvic canals than males, which the authors interpret as a likely adaptation to facilitate giving birth. Consequently, female pelvic morphology represents a functional trade-off between the narrowness required for efficient species-specific locomotion and the width necessary for giving birth to offspring (Csanády et al. 2019).

Sexual dimorphism of the pelvis has also been studied in rodents, where dimorphism is attributed to hormones and ontogeny (Gardner 1936; Bernstein and Crelin 1967; Uesugi et al. 1992). In laboratory rats, for example, sexual maturity occurs around six weeks of age (Sengupta 2013), and the first dimorphic features appear at 32 days of age (Bernstein and Crelin 1967). When comparing rats to laboratory mice, they found the biggest difference in pelvic sexual dimorphism was the pelvic canal size, which is greater in mice (wider female pelvic canal) compared to rats (Bernstein and Crelin 1967).

In laboratory house mice (*Mus musculus* or *domesticus*), pelvic shape and size are significantly modified by parity (the history of giving birth), with parous females having the largest os coxae (Schutz et al. 2009a). These parous females exhibit more divergent pelvic shapes relative to males than nulliparous females, with the puboischial complex representing the primary region of dimorphic change (Schutz et al. 2009a).

1.4. Study System

Detecting subtle functional adaptations remains challenging because environmental stochasticity and phylogenetic constraints introduce significant statistical noise across comparative analyses. To delineate the biomechanical effects of locomotion more clearly, controlled experimental frameworks are required, as can be achieved through artificial selection experiments (Rose and Garland, Jr. 2009). The High-Runner (HR) mouse experiment serves as a primary organismal model for evaluating the correlated responses to selection for high intensity locomotor behavior under replicated and highly controlled conditions (Swallow et al. 1998, 2009). Begun from an outbred (genetically variable) founding population of laboratory house mice in 1993, the protocol utilizes four replicate HR lines selectively bred for increased voluntary wheel running distance on days five and six of a six day trial as young adults, while four additional lines are maintained as non-selected controls (Swallow et al. 1998).

Increased wheel-running behavior (both daily distance and running speeds) in the HR lines leads to altered mechanical loading and would be expected to engender correlated responses in functionally relevant aspects of the skeleton.

Long-term artificial selection for voluntary exercise has elicited a suite of correlated behavioral, physiological, and morphological responses. Compared to non-selected Control mice, individuals from the HR lines have:

1. Elevated spontaneous physical activity (SPA) in home-cage environments when running wheels are not provided (Malisch et al. 2009; Khan et al. 2024).
2. Systematic reductions in adult body mass and body length, largely driven by decreased post-weaning growth rates (Swallow et al. 1999; Thompson et al. 2024).
3. Reduced adiposity (body fat mass), alongside an enhanced physiological capacity to conserve fat when faced with the acute energetic challenge of wheel running (Hiramatsu and Garland, Jr. 2018).
4. Superior aerobic performance, characterized by higher treadmill endurance and significantly elevated maximal oxygen consumption VO_2max during forced exercise (Meek et al. 2009; Schwartz et al. 2023).
5. Cardiac adaptations, including larger heart mass relative to body mass (Copes et al. 2015; Schwartz and Garland, Jr. 2024).

6. Larger femoral heads, which likely serve as a biomechanical adaptation to increase articular surface area at the hip, thereby reducing joint stress during loading (Garland, Jr. and Freeman 2005; Kelly et al. 2006; Castro and Garland, Jr. 2018).
7. Modular adaptations of the ribcage, including significant alterations in rib shape, count, and craniocaudal patterning within the thoracic region (Webb et al. 2026).
8. Divergent pelvic and hindlimb size and/or shape, including more gracile pelvic structures characterized by thinner distal ilia and lighter overall pelvic mass (Castro et al. 2021). Furthermore, µCT analyses demonstrate that exercise-induced loading via 13 weeks of voluntary wheel running (in these lines results in an increase in ilium cortical area (Lewton et al. 2019).

1.6. Hypotheses

Here, we studied the pelvic girdle of the HR mice from generation 93. Our first, general hypothesis was that the pelvis would differ in size (relative to body size) and/or multivariate shape between HR and C lines of mice. Second, we expected differences between males and females. Third, we expected that any differences would be greater in males than in females because the former are not constrained by the need to give birth. Finally, we expected to find evidence for

the evolution of "multiple solutions" among the four replicate High Runner lines (see Discussion).

2. Methods

2.1. Organismal Model and Selection Regime

The specimens utilized in this investigation were retired breeders from generation 93 of the High-Runner (HR) mouse selection experiment, an ongoing study of the evolution of voluntary exercise behavior initiated in 1993 (Swallow et al. 1998; Careau et al. 2013). Briefly, the founding population consisted of 224 outbred, genetically heterogeneous Hsd:ICR house mice (*Mus domesticus*), which were randomly mated for two generations before being partitioned into eight closed lines. Four of these replicate lines are selectively bred for high voluntary wheel-running distance, while the remaining four lines serve as non-selected controls. Selection is based on the total number of wheel revolutions recorded during the final two days of a six-day trial once individuals reach sexual maturity (~6–8 weeks of age) (Swallow et al. 1998). Within the HR lines, the highest-running male and female from each of the 10 families per line are chosen as breeders, whereas breeders for the Control lines a male and female from within each family are chosen at random (Swallow et al. 1998). To reduce inbreeding, sibling matings are prohibited (Swallow et al. 1998). Throughout the

experiment, mice are maintained on a 12:12-hour light:dark cycle with ad libitum access to water and a standard laboratory rodent diet (Harlan Teklad [W]-8604). Following a 19-day co-housing period for breeding, pregnant dams are transitioned to a high-nutrient breeder diet (Harlan Teklad [S-2335]-7004) until offspring reached weaning at post-natal day 21.

2.2. Specimens

The specimens analyzed in the present study (100 males, 95 females; Table 1) are the same as used by Webb et al. (2026) in their investigation of thoracic morphology. Males were euthanized at a mean age of 95 days, following their removal from breeding pairs, while females were sacrificed at an average of 126 days, exactly seven days after their pups were weaned at 21 days of age. This specific timeline for females is important for pelvic analysis, as the history of parturition (parity) is known to induce significant changes in the murine puboischial complex (Schutz et al. 2009a). Immediately following sacrifice via carbon dioxide inhalation, body mass was recorded to the nearest 0.01 g and body length (rostrum to anus) was measured to the nearest mm (Webb et al. 2026).

2.3. Three-Dimensional µCT Analysis and Reconstruction

As described previously, carcasses were stored at -20°C prior to postmortem imaging. High-resolution three-dimensional (3D) pelvic volumes were captured using a Nikon XT225ST µCT scanner (80 kV, 120 uA, 1440 projections), yielding scans with an isometric pixel size of 61 µm (Webb et al. 2026). The pelvic skeletal elements were digitally isolated from the surrounding soft tissue using Dragonfly ORS (v. 2022.1; Comet Technologies, Canada). The resulting osteological meshes were converted into 3D surface wraps in MeshLab (v. 2022.02) utilizing Poisson surface reconstruction (Cignoni et al. 2008; Kazhdan and Hoppe 2013).

2.4. Statistical Analysis of Body Size and Pelvis Centroid Size

In accordance with established protocols for the HR model, phenotypic traits were analyzed using SAS Procedure MIXED (SAS Institute, Cary, NC) (e.g., Copes et al. 2015; Castro and Garland, Jr. 2018; Hiramatsu and Garland, Jr. 2018; Schwartz and Garland, Jr. 2024). The statistical models employed sex and 'linetype' (HR vs. Control) as fixed effects, with replicate line nested within linetype as a random effect (Castro and Garland, Jr. 2018; Webb et al. 2026). Degrees of freedom for testing the main effects of linetype, sex, and their interaction were 1 and 6. Because the mammalian pelvis scales significantly with

body size, body length was used a covariate to control for allometric effects on pelvic architecture (Martín-Serra et al. 2014; Lewton et al. 2020). We allowed for different variances between HR and C groups, both at the level of among lines and at the level of residual variation.

2.5. Pelvis Isolation, Landmark Collection, Visualization, and Statistical Analyses

Pelvis morphology was quantified using 3D geometric morphometrics (Zelditch et al. 2026). A total of 44 homologous landmarks were digitized for each pelvis specimen using 3D Slicer software, version 5.8.1 (Kikinis et al. 2014). The 3D surface wraps (.stl files) created in Webb et al. (2026) were imported into 3D Slicer (https://www.slicer.org/), where a Region of Interest (ROI) was placed to encapsulate the pelvis. The ROI was then clipped to create a new model, removing the rest of the mouse skeleton. The online Supplemental Files includes a complete description of the procedures used to process scans and place landmarks (Supplementary_Material_Protocol 3dslicer_V10ProQuest.docx).

Based on the landmarks from Berdnikovs et al. 2007, Waltenberger et al. 2021, and Özkan et al 2024, 44 landmarks were chosen to capture the overall shape of the pelvis. With the isolated pelvis, the 44 landmarks were placed on

100 male and 95 female specimens (two males and three females were subsequently excluded from analyses as outliers: see below). The 3D coordinates for the 44 landmarks were then exported as a csv file for each mouse. Custom R code was then used to read in these files and create a single csv file containing all mice.

Shape analysis was performed using the R package geomorph (Baken et al. 2021). To align landmarks within a common shape space and eliminate the effects of translation, rotation, and size, a generalized Procrustes superimposition (GPA) was executed via the ‘gpagen’ function (Rohlf and Slice 1990; Zelditch and Swiderski 2024).

Principal components (N = 125) were computed from the 44 landmark coordinates. Principal component (PC) scores for the first four axes were extracted for each individual and used to visualize morphospace occupation. To illustrate the extent of morphospace occupied by each line, convex hull polygons were calculated from the PC scores using the chull() function and overlaid onto the PC scatterplots. Figures were generated using the ggplot2 package in R. Based on scatterplots of scores for PCs 1 through 4, we identified five outliers (96200 F, 96332 F, 96013 F, 96233 M, 96012 M), i.e., specimens whose scores were discrepant relative to their sex and linetype minimum convex polygons (96200 and 96332). Three of these individuals had apparent deformities or

dubious scans (96233, 96012, 96013). These five individuals were removed from the dataset, resulting in 98 males and 92 females.

Statistical analyses used Procrustes coordinates as the dependent variable, with replicate line nested within linetype. To control for allometry, body length was included as a covariate (Klingenberg 2016), as this measure has been demonstrated to be a superior predictor of skeletal morphology in High Runner (HR) mice compared to body mass (Castro et al. 2021). Statistical models were implemented via the 'procD.lm' function of geomorph using 10,000 iterations and Type III Sums of Squares. The use of Type III Sums of Squares aligns with the established conventions of the HR mouse experiment, as in the SAS analyses described above. This method is unaffected by the order of factors and effectively handles uneven sample sizes. Finally, to account for the fact that each replicate line represents an independent experimental iteration, the 'anova' function was used to adjust error effects. This ensured that the effect of linetype was evaluated relative to the variance associated with the replicate lines rather than the residual error, with 1 and 6 d.f.). The online supplemental **Supplemental Files** includes a complete output with all R code and Results, as a Microsoft Word file (PelvisShape_Analysis_Code_40_Supp.docx).

3. Results

3.1. Body Length

Considering both sexes, body length did not significantly differ between HR and Control lines (**Table 2A**) (SAS Procedure Mixed with REML estimation and Type III tests of fixed effects: N=190, Flinetype=1.98, d.f.=1,6, p=0.2095; Least Squares Means and associated Standard Errors were 10.90±0.07mm for Control and 10.75±0.08mm for HR lines). By contrast, the effect of sex was significant (Fsex=15.00, d.f.=1,6, p=0.0082), with LSM ± SE of 10.91±0.06 mm for females and 10.74±0.06 mm for males. The sex-by-linetype interaction term was non-significant (Fsex∗linetype=0.05, d.f.=1,6, p=0.8313). Considering the sexes separately, body length did not significantly differ between the two linetypes for either females (**Table 2B**) or males (**Table 2C**).

Body length differed among genetic lines and between sexes **(Fig. 3A).** Across both Control and High Runner lines, females generally exhibited greater least-squares mean body lengths than males. Variation among genetic lines was evident within both line types, with Co4 and HR8 exhibiting the largest body

lengths and HR6 and HR7 exhibiting comparatively smaller body lengths. Individual variation within each line and sex is shown by the distribution of gray points.

3.2. Pelvis Centroid Size

With body length as a covariate ($F_{length}=95.49$, d.f.=1, 173, $p<0.0001$), HR and Control lines did not significantly differ for centroid size (N=190, $F_{linetype}=0.72$, d.f.=1,6, $p=0.4286$) (**Table 2D**). By contrast, the effect of sex was highly significant ($F_{sex}=401.52$, d.f.=1,6, $p<0.0001$), with females having larger centroid sizes than males. The sex-by-linetype interaction term was non-significant ($F_{sex*linetype}=0.06$, d.f.=1,6, $p=0.8144$). Considering the sexes separately, HR and Control lines did not significantly differ for either females (**Table 2E**) or males (**Table 2F**).

After adjusting for body length as a covariate, pelvis centroid size also varied among genetic lines and between sexes **(Fig. 3B)**. Females generally exhibited larger adjusted centroid sizes than males across both Control and High Runner lines. Among the Control lines, Co2 and Co4 had the largest adjusted centroid sizes, whereas HR8 exhibited the largest adjusted centroid size among the High Runner lines. Differences among genetic lines remained evident after accounting for body length.

3.3. Pelvis Shape

Pelvis Shape for Both Sexes

Using all mice for the pelvis with no covariate (**Table 3A**), selective breeding for high voluntary activity significantly impacted shape (Nested Procrustes ANOVA with Type III Sums of Squares: N=190, Flinetype=32.03, d.f.=1,174, Z=4.86 p=0.0001). Sexual dimorphism in overall pelvic morphology was highly significant (Fsex=41.90, d.f.=1,174, Z=6.10, p=0.0001), although the sex-by-linetype interaction term was non-significant (Fsex∗linetype=0.15, d.f.=1,174, p=0.8336). Regarding variation among the replicate lines (nested within linetype), the overall pelvis shape varied significantly (Fline(linetype)=12.95, d.f.=6,174, Z=7.05, p=0.0001). These replicate lines accounted for a larger portion of the total morphological variation in the model (R^2=0.096) than the effect of selection for running behavior itself. The interaction between replicate line and sex was non-significant (Fline(linetype)∗sex=1.54, d.f.=6,174, p=0.1230).

Results were similar with body length as a covariate, which was not a significant predictor of pelvis shape (**Table 3B**). Results were also similar with centroid size as a covariate, although it was a significant predictor of pelvis shape (**Table 3C**).

Shape by Line

Using the High Runner subset for the pelvis with no covariate (**Table 4A**), replicate line significantly impacted shape (Procrustes ANOVA with Type III Sums of Squares: N=99, FLine=23.40, d.f.=3, 91, Z=6.68, p=0.0001). Sexual dimorphism in overall pelvic morphology was highly significant (FSex=47.09, d.f.=1, 91, Z=6.03, p=0.0001), although the line-by-sex interaction term was non-significant (FLine×Sex=1.98, d.f.=3, 91, p=0.0860). Regarding variation among the replicate lines, the overall pelvis shape varied significantly (FLine=23.40, d.f.=3, 91, Z=6.68, p=0.0001). These replicate lines accounted for a larger portion of the total morphological variation in the model (R^2=0.141) than the effect of sexual dimorphism itself (R^2=0.095). Finally, the interaction between replicate line and sex was non-significant (FLine×Sex=1.98, d.f.=3, 91, p=0.0860).

Using the Control subset for the pelvis with no covariate (**Table 4B**), replicate line significantly impacted shape (Procrustes ANOVA with Type III Sums of Squares: N=91, FLine=2.89, d.f.=3, 83, Z=2.04, p=0.0201). Sexual dimorphism in overall pelvic morphology was highly significant (FSex=41.03, d.f.=1, 83, Z=6.00, p=0.0001), although the line-by-sex interaction term was non-significant (FLine×Sex=1.10, d.f.=3, 83, p=0.3542). Regarding variation among

the replicate lines, the overall pelvis shape varied significantly (FLine=2.89, d.f.=3, 83, Z=2.04, p=0.0201). In this control group, these replicate lines accounted for a smaller portion of the total morphological variation in the model (R^2=0.031) than the effect of sexual dimorphism itself (R^2=0.148). Finally, the interaction between replicate line and sex was non-significant (FLine×Sex=1.10, d.f.=3, 83, p=0.3542).

Results were similar with body length as a covariate for both HR and C, which was not a significant predictor of pelvis shape (**Table 4C** for HR and **Table 4D** for C mice). Results were also similar with centroid size as a covariate for both HR and C, although it was a significant predictor of pelvis shape (**Table 4E** for HR and **Table 4F** for C mice).

Shape by Females

Males and females were analyzed both together and separately because females were older at the time of sacrifice, had experienced pregnancy and parturition, and show significant sexual dimorphism in skeletal traits associated with the hindlimb (Castro and Garland, Jr. 2018). Using the female subset for the pelvis with no covariate (**Table 5A**), selective breeding for high voluntary activity significantly impacted shape (Nested Procrustes ANOVA with Type III Sums of Squares: N=92, FLinetype=24.88,

d.f.=1, 84, Z=4.43, p=0.0001). Pelvis shape also varied significantly among lines (FLine(Linetype)=10.06, d.f.=6, 84, Z=6.24, p=0.0001). These replicate lines accounted for a substantially larger portion of the total morphological variation in the model (R^2=0.362) than the effect of selection for running behavior itself (R^2=0.149).

Results were similar with body length as a covariate for all females, which was not a significant predictor of pelvis shape (**Table 5B**). Results were also similar with centroid size as a covariate for all females, although it was a significant predictor of pelvis shape (**Table 5C**).

Shape by Males

Using the male subset for the pelvis with no covariate (**Table 6A**), selective breeding for high voluntary activity significantly impacted shape (Nested Procrustes ANOVA with Type III Sums of Squares: N=98, FLinetype=43.39, d.f.=1, 90, Z=4.58, p=0.0001). Regarding variation among the replicate lines (nested within linetype), the overall pelvis shape varied significantly (FLine(Linetype)=28.07, d.f.=6, 90, Z=8.80, p=0.0001). These replicate lines accounted for a substantially larger portion of the total morphological variation in the model (R^2=0.605) than the main effect of selection for running behavior itself (R^2=0.156).

Results were similar with body length as a covariate for all males, which was not a significant predictor of pelvis shape (**Table 6B**). Results were also similar with centroid size as a covariate for all Males, although it was a significant predictor of pelvis shape (**Table 6C**).

Shape by Female HR Lines

Using the female High Runner (HR) subset for the pelvis with no covariate (*Table 7A*), replicate line significantly impacted shape (Procrustes ANOVA with Type III Sums of Squares: N=47, FLine=15.18, d.f.=3, 43, Z=5.08, p=0.0001). Regarding variation among these four selected lines, the overall pelvis shape varied significantly (FLine=15.18, d.f.=3, 43, Z=5.08, p=0.0001). Within this female HR group, these replicate lines accounted for a substantial portion of the total morphological variation in the model (R^2=0.514), representing over half of the observed shape variance.

Results were similar with body length as a covariate for HR females, which was not a significant predictor of pelvis shape (**Table 7B**). Results were also similar with centroid size as a covariate for HR females, although it was a significant predictor of pelvis shape (**Table 7C**).

Shape by Female C Lines

Using the female Control subset for the pelvis with no covariate (**Table 8A**), replicate line significantly impacted shape (Procrustes ANOVA with Type III Sums of Squares: N=45, FLine=2.81, d.f.=3, 41, Z=2.03, p=0.0205). Regarding variation among these four control lines, the overall pelvis shape varied significantly (FLine=2.81, d.f.=3, 41, Z=2.03, p=0.0205). Within this female control group, these replicate lines accounted for a moderate portion of the total morphological variation in the model (R^2=0.171). While significant, this is a smaller portion of the variance than seen in the female HR lines (R 2=0.514), likely reflecting the absence of directional selection for wheel-running behavior.

Results were similar with body length as a covariate for C females, which was not a significant predictor of pelvis shape (**Table 8B**). Results were also similar with centroid size as a covariate for C females, although it was a significant predictor of pelvis shape (**Table 8C**).

Shape by Male HR Lines

Using the male High Runner (HR) subset for the pelvis with no covariate (**Table 9A**), replicate line significantly impacted shape (Procrustes ANOVA with

Type III Sums of Squares: N=52, FLine=74.61, d.f.=3, 48, Z=9.02, p=0.0001; R^2=0.823). Regarding variation among these replicate lines, the overall pelvis shape varied significantly (F Line=74.61, d.f.=3, 48, Z=9.02, p=0.0001). These replicate lines accounted for a larger portion of the total morphological variation in the model (R^2=0.823) than observed in the female HR or control subsets.

Results were similar with body length as a covariate for HR males, which was not a significant predictor of pelvis shape (**Table 9B**). Results were also similar with centroid size as a covariate for HR males, which was **not** a significant predictor of pelvis shape (Table 9C).

Shape by Male C Lines

Using the male Control subset for the pelvis with no covariate (**Table 10A**), replicate line significantly impacted shape (Procrustes ANOVA with Type III Sums of Squares: N=46, FLine=3.48, d.f.=3, 42, Z=2.06, p=0.0180). Regarding variation among these replicate lines, the overall pelvis shape varied significantly (FLine=3.48, d.f.=3, 42, Z=2.06, p=0.0180). These replicate lines accounted for a moderate portion of the total morphological variation in the model (R^2=0.199).

Results were similar with body length as a covariate for C males, which

was not a significant predictor of pelvis shape (**Table 10B**). Results were also similar with centroid size as a covariate for C males, which was **not** a significant predictor of pelvis shape (**Table 10C**).

4. Discussion

Overall Findings in Relation to Hypotheses

The mechanical demands of locomotion and those related to reproduction may often conflict (e.g., Hogervorst et al. 2009; Ricklan et al. 2021). More generally, evolutionary trajectories of all traits are shaped by trade-offs, where, for example, the enhancement of one function occurs at a physiological or biomechanical cost to another (Garland, Jr. et al. 2022). As outlined in the Introduction, the mammalian pelvis is one structure where such conflicts and trade-offs may be particularly apparent. Here, we studied the High Runner (HR) mouse model (Garland, Jr. 2003; Swallow et al. 2009; Wallace and Garland, Jr. 2016) to four hypotheses. Our first hypothesis, that pelvis shape would differ between the 4 selectively bred High Runner lines and their 4 non-selected Control lines, was supported. Our second hypothesis was also supported: pelvis shape differs strongly between male and female mice. Our third hypothesis was that HR vs C differences would be greater in males than females because the former are not constrained by the need to give birth. This was not supported, as we found no statistically significant sex-by-linetype interaction. Finally, as hypothesized, we found that the HR lines have diverged in morphospace from

each other, and more than have the C lines, providing evidence for multiple solutions (adaptive responses) to uniform selection.

Based on analysis of PC scores (Table 3), HR and C lines of mice are strongly separated in pelvic morphospace (as indicated by Z scores in the range of 3.6-4.9), even when accounting for potential associations with pelvic centroid size or body length. Thus, our first hypothesis was supported. In addition, we found that the female and male pelvis occupy separate areas in morphospace (e.g., see Figures 4 and 5), including in analyses with body size or pelvis centroid size as covariates (Table 3). Some of this differentiation could be caused by females having given birth (and potentially by the females being older than males). However, given the magnitude of the sex differences (Z scores in the range of 4.5-6.1), we believe that it largely reflects inherent biological differences between the sexes. Results from the present study are consistent with previous reports of sexual dimorphism in the pelvic girdle of mice (Uesugi et al. 1992; Berdnikovs 2007; Schutz et al. 2009).

We did not, however, find evidence for a linetype-by-sex interaction (Table 3). Therefore, our second hypothesis that linetype differences beween the sexes would be smaller for females -- because their pelvic evolution in response to selective breeding for endurance running may be constrained by reproductive demands -- was not supported. Pelvis centroid size (with body length as a

covariate: Table 2) differed between the sexes (females larger) but not between linetypes, and we again found no linetype*sex interaction. Note that body length was significantly longer in females than males, with no statistically significant effect of linetype and no linetype*sex interaction (Table 2). Thus, the response to selection was specific to pelvic shape rather than pelvic size or overall body size, a finding consistent with Webb et al. (2026), who studied the ribs. Taken together, our results and those of Webb et al. (2026) indicate that the response of the axial skeleton to selection for high voluntary activity has involved morphological reorganization, specifically overall shape changes in the pelvis and ribs, along with changes in structural patterning in the ribcage (e.g., rib counts), rather than changes in overall skeletal size.

Multiple Solutions and Many-to-One Mapping

A key finding of this study is the greater variation among the four replicate HR lines than among the four Control lines (Tables 7-10). This high degree of dispersion among HR lines in morphospace (e.g., Figures 6, 7) indicates that each line evolved its pelvic shape somewhat differently. These results suggest that redundant or "many-to-one mapping" (Alfaro et al. 2004) has allowed the evolution of "multiple solutions" to uniform selection in the HR lines. As noted by Wainwright et al. (2005), many-to-one mapping is a “ubiquitous feature of biological design” that allows for redundant mapping between underlying features

and whole-organism performance. This redundancy explains how different combinations of skeletal dimensions, such as the varying hind limb dimensions in lizards that produce similar jumping abilities (Toro et al. 2004) or the diverse combinations of leg length and muscle mass in anurans that yield equivalent jumping and swimming performance (Moen 2019). A finding of greater dispersion in morphospace for the HR versus non-selected Control lines is consistent with the findings of Webb et al. (2026) in the ribcage. Various other examples of multiple solutions, including for running behavior itself (Garland, Jr. et al. 2011; Hillis and Garland 2023) and muscle properties (Castro and Garland, Jr. 2018), have been reported.

Our findings for the HR lines contrast with the macroevolutionary results of Martín-Serra et al. (2014), who described the carnivoran appendicular skeleton as an example of a “one-to-many” pattern between phenotype and function, and a general lack of correspondence between locomotor type and skeletal phenotype (see also Lewton et al. 2020). These functional signals of adaptation may be obscured by deep-time phylogenetic associations or constraints (e.g., see Blomberg and Garland, Jr. 2002; Blomberg et al. 2003).

The specific "solutions" reached by each line likely reflect their genetic backgrounds to some extent. For instance, the "mini-muscle" phenotype, which became fixed in HR Line 3 and remains polymorphic in Line 6 (e.g., see Garland,

Jr. et al. 2002; Dlugosz et al. 2009; Castro et al. 2024), illustrates how specific genetic mutations can influence morphological and physiological outcomes. The distinct morphospace occupied by Line 3 (Figures 6, 7) may therefore represent a pelvic adaptation specifically associated with this unique mutation.

Modular Adaptation: Birth vs. Locomotion

The mammalian pelvis is a complex, multi-bone structure comprising the ilium, ischium, pubis, and sacrum. Although the present study analyzed overall pelvic shape through 3D geometric morphometrics rather than individual bone measurements, these distinct elements play specialized roles in weight bearing, muscle attachment, and parturition. Consequently, shape changes in specific regions can reveal locomotor responses to selection for high activity (voluntary wheel-running) or sexual dimorphism. The TPS grids (Figures 4B and 5B) allow for the visualization of these localized changes along the primary axes of variation.

Obstetric Module and Sexual Dimorphism

Analysis of the principal components shows that PC1 primarily captures the significant sexual dimorphism inherent in the pelvic girdle. As illustrated by

the TPS grids (Figure 4), the "PC1 max" position, occupied by females, features a noticeably wider region for the pelvic canal, defined by the expansion of the pubis and ischium and a wider orientation of the sacrum. This anatomical configuration is consistent with the "obstetric module" described by Ricklan et al. (2021), which encompasses the dimensions necessary to facilitate the passage of neonates.

Locomotor Adaptations and the Cursorial Hypothesis

In our original hypotheses, we expected HR mice to evolve a "longer and narrower" pelvis, mirroring the specialized morphology seen in cursorial specialists like the cheetah or canids, and even terrestrial spiny rats (Martín-Serra et al. 2014; Tavares and Pessôa 2020; Pallandre et al. 2021). However, the HR and C lines did not differ statistically (results not shown) for any of the first four PCs (Figures 4, 5), whereas examination of the TPS grids reveals more nuanced anatomical changes. Specifically, while PC1 emphasizes sexual dimorphism, PC2 captures variation in the distance of the ilium (specifically the ilia wing) from the sacrum (Figure 4).

However, certain bones within the pelvis have been shown to be more sensitive to selective breeding, showing trends toward a more gracile structure, such as the thinner distal ilia previously noted in these lines by Castro et al.

(2021). Moreover, mice with the mini-muscle phenotype (all of HR line 3 and some within line 6) have clearly longer and thinner hindlimbs (e.g., see Kelly et al. 2006).

Caveats, Limitations, and Future Directions

Although the 3D geometric morphometric techniques used in this study provide an important step towards the assessment of pelvic shape, several caveats regarding our experimental design and sample must be addressed. Specifically, although our overall morphometric patterns reveal clear divergence between the replicate lines, further analysis of the existing µCT scans could provide a more granular look at the individual pelvic bone dimensions that contribute to these overarching shapes.

Methodological Refinements and Linear Measurements

We used landmark-based 3D geometric morphometrics to study overall pelvic shape. Other methods for data collection have been used in previous studies, including 2D geometric morphometrics (e.g., Álvarez et al. 2013), angle measurements (e.g., Pallandre et al. 2021), and linear measurements (e.g., Tavares and Pessôa 2020). Each of the methods has their advantages and disadvantages. For example, 2D geometric morphometrics has the advantage of

using economic photo capturing, ideal for flat anatomical features, and reduced dimensionality for data analysis. However, in a 2D space, non-flat anatomical features can be distorted, also leading to less precise landmark placement, and data analysis is limited to reduced dimensionality (Zelditch et al. 2026). Second, linear measurements do not show the overall shape, but the advantage is that they are interpretable individually, and also sometimes as functional ratios (Zelditch et al. 2026). Lastly, although angle measurement can provide information that is rather directly related to biomechanical performance, specifically where the bones are in relation to an anatomical point, the shape of the bones measured will remain unknown.

To complement our geometric morphometric analysis, future research should incorporate precise linear measurements of the pelvic canal. Specifically, utilizing existing landmarks to calculate the distance between the left and right sides (e.g., landmarks 43/44 and 16/17) would provide a numerical assessment of canal width to validate our shape-based findings. Alternatively, analyzing functional ratios of linear dimensions (including ratios to the hindlimbs bones), specifically the ratio of ischium and pubis width to the total length of the innominate bone (os coxae), would provide a standardized measure of pelvic proportions. Such individual bone measurements would help clarify the exact extent to which the HR pelvis is "narrower" or "longer," building on historical descriptions of rodent pelvic dimorphism, such as Gardener’s (1936) work on

house mice and Dunmire's multispecies study (1955). Additionally, measuring the width of the sacrum (e.g., distance between landmarks 41 and 42) would allow for a more integrated analysis of the pelvic ring. This would also add to the skeletal connectivity of the vertebrae currently under investigation by Hennekam et al. (personal communication).

Sampling and Phenotypic Plasticity

It is important to acknowledge that the specimens utilized in this investigation, retired breeders from generation 93, were chosen partly to economize on animal usage within the long-term experiment. Consequently, we cannot fully disentangle genetically fixed traits from the phenotypic plasticity (or "adaptation") induced by a lifetime of mechanical loading during normal locomotion within cages (plus 6 days of wheel access) and the possibly permanent remodeling associated with reproduction and birth. In laboratory house mice, the male pelvis is more different compared to parous females than when compared to nulliparous females, which likely accounts for a portion of our observed sexual dimorphism (e.g., Uesugi et al. 1992; Berdnikovs et al. 2007; Schutz et al. 2009a). Furthermore, because loading and joint forces result in continuous change in the pelvis (Siegel and Jones 1975; Lionberger et al. 1985), a future study conducted across ontogeny for the HR mice would be critical to

identifying the developmental point at which selective and dimorphic features first emerge (Bernstein and Crelin 1967).

Integrative Analyses of Skeletal Evolution

Future directions should also investigate how pelvic shape correlates with the wider axial skeleton; for instance, Esteban et al. (2020) demonstrated that sacrum morphology is significantly related to relative tail length in Carnivora, suggesting that tail dimensions should be included in future, synthetic analyses of skeletal evolution.

Acknowledgments

Supported by NSF grant IOS-2038528, a Butterfly Project Fellowship, and a P.O.D.E.R Scholarship.

Tables

Table 1 – Sample Size for Control and High Runner Mice.

Linetype	Control				High Runner			
Line	1	2	4	5	3	6	7	8
Sex	F M	F M	F M	F M	F M	F M	F M	F M
Number of Specimens	10 11	12 12	11 12	12 11	12 12	11 16	12 12	12 12

Abbreviations: F, Female; M, Male.

190 total=98 males + 92 females

Control females: 45

Control males: 46

HR females: 47

HR males: 52

Grand total: 45 + 46 + 47 + 52=190 specimens.

Table 2 – Body Length and Centroid Size from SAS

Table 2A Body Length by Sex and Linetype

Covariance Parameter Estimates

Cov Parm	Group	Estimate	Standard Error	Z Value	Pr > Z
Line(Linetype)	**Linetype 0**	0.01442	0.01419	1.02	0.1547357494
Line(Linetype)	**Linetype 1**	0.02105	0.02173	0.97	0.1663048401
Sex*Line(Linetype)	**Linetype 0**	0	.	.	.
Sex*Line(Linetype)	**Linetype 1**	0.006280	0.008166	0.77	0.2209454582
MouseI(Linetyp*Line)	**Linetype 0**	0.06508	0.009926	6.56	<.0000000001
MouseI(Linetyp*Line)	**Linetype 1**	0.04567	0.006767	6.75	<.0000000001

Type 3 Tests of Fixed Effects

Effect	Num DF	Den DF	F Value	Pr > F
Sex	1	6	14.998118733	0.0082396723
Linetype	1	6	1.9750484866	0.2095197087
Sex*Linetype	1	6	0.0494964683	0.8313216985

Least Squares Means

Effect	Sex	Linetype	Estimate	Standard Error	DF	t Value	Pr > |t|
Sex	**0**		10.9113	0.05670	6	192.43	<.0000000001
Sex	**1**		10.7396	0.05645	6	190.27	<.0000000001
Linetype		**0**	10.8986	0.06574	6	165.77	<.0000000001
Linetype		**1**	10.7523	0.08071	6	133.23	<.0000000001
Sex*Linetype	**0**	**0**	10.9894	0.07110	6	154.56	<.0000000001
Sex*Linetype	**0**	**1**	10.8332	0.08835	6	122.61	<.0000000001
Sex*Linetype	**1**	**0**	10.8078	0.07086	6	152.52	<.0000000001
Sex*Linetype	**1**	**1**	10.6713	0.08788	6	121.43	<.0000000001

Table 2B. Body Length by Linetype for Females

Covariance Parameter Estimates

Cov Parm	Group	Estimate	Standard Error	Z Value	Pr > Z
Line(Linetype)	**Linetype 0**	0.01311	0.01646	0.80	0.2130163631
Line(Linetype)	**Linetype 1**	0.02304	0.02256	1.02	0.1535623252
MouseI(Linetyp*Line)	**Linetype 0**	0.07270	0.01608	4.52	0.0000030986
MouseI(Linetyp*Line)	**Linetype 1**	0.05449	0.01175	4.64	0.0000017614

Type 3 Tests of Fixed Effects

Effect	Num DF	Den DF	F Value	Pr > F
Linetype	1	6	2.0463036398	0.2025247087

Least Squares Means

Effect	Linetype	Estimate	Standard Error	DF	t Value	Pr > |t|
Linetype	**0**	10.9894	0.06998	6	157.03	<.0000000001
Linetype	**1**	10.8339	0.08319	6	130.23	<.00000000

Table 2C. Body Length by Linetype for Males

Covariance Parameter Estimates

Cov Parm	Group	Estimate	Standard Error	Z Value	Pr > Z
Line(Linetype)	**Linetype 0**	0.01479	0.01623	0.91	0.1810873418
Line(Linetype)	**Linetype 1**	0.03085	0.02749	1.12	0.1308395397
MouseI(Linetyp*Line)	**Linetype 0**	0.05824	0.01271	4.58	0.0000022912
MouseI(Linetyp*Line)	**Linetype 1**	0.03781	0.007716	4.90	0.0000004785

Type 3 Tests of Fixed Effects

Effect	Num DF	Den DF	F Value	Pr > F
Linetype	1	6	1.3933750917	0.2825073584

Least Squares Means

Effect	Linetype	Estimate	Standard Error	DF	t Value	Pr > |t|
Linetype	**0**	10.8092	0.07047	6	153.39	<.0000000001
Linetype	**1**	10.6725	0.09193	6	116.10	<.0000000001

Table 2D. Centroid Size with Body Length as a Covariate by Sex and Linetype

Covariance Parameter Estimates

Cov Parm	Group	Estimate	Standard Error	Z Value	Pr > Z
Line(Linetype)	**Linetype 0**	1.0843	0.9465	1.15	0.1259735677
Line(Linetype)	**Linetype 1**	1.6566	1.3714	1.21	0.1135286373
Sex*Line(Linetype)	**Linetype 0**	0.08833	0.1134	0.78	0.2180087357
Sex*Line(Linetype)	**Linetype 1**	0	.	.	.
MouseI(Linetyp*Line)	**Linetype 0**	0.5716	0.08899	6.42	<.0000000001
MouseI(Linetyp*Line)	**Linetype 1**	0.5235	0.07653	6.84	<.0000000001

Type 3 Tests of Fixed Effects

Effect	Num DF	Den DF	F Value	Pr > F
Sex	1	6	401.51844353	0.0000010029
Linetype	1	6	0.7201512331	0.4286456325
Sex*Linetype	1	6	0.0601979925	0.8143598390
LENGTH	1	173	95.487484637	<.0000000001

Least Squares Means

Effect	Sex	Linetype	Estimate	Standard Error	DF	t Value	Pr > |t|
Sex	**0**		47.4484	0.4281	6	110.83	<.0000000001
Sex	**1**		44.3260	0.4276	6	103.67	<.0000000001
Linetype		**0**	46.2445	0.5374	6	86.05	0.0000000002
Linetype		**1**	45.5299	0.6479	6	70.28	0.0000000006
Sex*Linetype	**0**	**0**	47.7872	0.5545	6	86.17	0.0000000002
Sex*Linetype	**0**	**1**	47.1096	0.6522	6	72.24	0.0000000005
Sex*Linetype	**1**	**0**	44.7017	0.5528	6	80.86	0.0000000002
Sex*Linetype	**1**	**1**	43.9502	0.6523	6	67.38	0.0000000007

Table 2E. Centroid Size with Body LLength as a Covariate by Linetype for Females

Covariance Parameter Estimates

Cov Parm	Group	Estimate	Standard Error	Z Value	Pr > Z
Line(Linetype)	**Linetype 0**	0.9053	0.7821	1.16	0.1235114261
Line(Linetype)	**Linetype 1**	1.7405	1.4708	1.18	0.1183355437
MouseI(Linetyp*Line)	**Linetype 0**	0.4782	0.1063	4.50	0.0000034457
MouseI(Linetyp*Line)	**Linetype 1**	0.7173	0.1549	4.63	0.0000018245

Type 3 Tests of Fixed Effects

Effect	Num DF	Den DF	F Value	Pr > F
Linetype	1	6	0.7885750993	0.4087161422
LENGTH	1	83	34.984450628	0.0000000716

Least Squares Means

Effect	Linetype	Estimate	Standard Error	DF	t Value	Pr > |t|
Linetype	**0**	48.0371	0.4875	6	98.55	<.0000000001
Linetype	**1**	47.2995	0.6716	6	70.43	0.0000000006

Table 2F. Centroid Size with Body Length as a Covariate by Linetype for Females

Covariance Parameter Estimates

Cov Parm	Group	Estimate	Standard Error	Z Value	Pr > Z
Line(Linetype)	**Linetype 0**	1.4591	1.2395	1.18	0.1195650966
Line(Linetype)	**Linetype 1**	1.4510	1.2122	1.20	0.1156410137
MouseI(Linetyp*Line)	**Linetype 0**	0.6541	0.1434	4.56	0.0000025301
MouseI(Linetyp*Line)	**Linetype 1**	0.3475	0.07124	4.88	0.0000005343

Type 3 Tests of Fixed Effects

Effect	Num DF	Den DF	F Value	Pr > F
Linetype	1	6	0.603029968	0.4669241895
LENGTH	1	89	70.117287678	<.0000000001

Least Squares Means

Effect	Linetype	Estimate	Standard Error	DF	t Value	Pr > |t|
Linetype	**0**	44.4589	0.6162	6	72.15	0.0000000005
Linetype	**1**	43.7861	0.6082	6	72.00	0.0000000005

Table 3— Shape ANOVA All Mice (No Covariate, with Length, with Centroid)

Table 3A. Pelvis Shape for Both Sexes (1N)

```
Analysis of Variance, using Residual Randomization
Permutation procedure: Randomization of null model residuals
Number of permutations: 10000
Estimation method: Ordinary Least Squares
Sums of Squares and Cross-products: Type III
Effect sizes (Z) based on F distributions

                   Df      SS        MS      Rsq       F       Z Pr(>F)
linetype            1 0.01787 0.0178744 0.039453 32.0339  4.8583 0.0001
sex                 1 0.02338 0.0233795 0.051604 41.9000  6.0966 0.0001
linetype:sex        1 0.00008 0.0000850 0.000188  0.1523 -0.9746 0.8336
linetype:line       6 0.04336 0.0072262 0.095700 12.9506  7.0507 0.0001
linetype:sex:line   6 0.00514 0.0008566 0.011345  1.5352  1.1558 0.1230
Residuals         174 0.09709 0.0005580 0.214298
Total             189 0.45306
---

Call: procD.lm(f1 = shape ~ linetype + sex + linetype * sex +
linetype/line +
    linetype/line * sex, iter = 9999, SS.type = "III", data = pca_gdf)
```

Table 3B. Pelvis Shape for Both Sexes with Length (1L)

```
Analysis of Variance, using Residual Randomization
Permutation procedure: Randomization of null model residuals
Number of permutations: 10000
Estimation method: Ordinary Least Squares
Sums of Squares and Cross-products: Type III
Effect sizes (Z) based on F distributions

                   Df      SS        MS      Rsq       F       Z Pr(>F)
linetype            1 0.01760 0.0175989 0.038845 31.4216  4.7510 0.0001
sex                 1 0.02278 0.0227763 0.050273 40.6654  5.9684 0.0001
length              1 0.00019 0.0001935 0.000427  0.3455 -0.4623 0.6760
linetype:sex        1 0.00008 0.0000760 0.000168  0.1358 -1.0446 0.8463
linetype:line       6 0.04200 0.0070008 0.092715 12.4994  6.9404 0.0001
linetype:sex:line   6 0.00483 0.0008051 0.010662  1.4374  0.9984 0.1588
Residuals         173 0.09690 0.0005601 0.213871
Total             189 0.45306
---

Call: procD.lm(f1 = shape ~ linetype + sex + linetype * sex +
linetype/line +
    linetype/line * sex + length, iter = 9999, SS.type = "III",
data = pca_gdf)
```

Table 3C. Pelvis Shape for Both Sexes with Centroid Size (1S)

```
Analysis of Variance, using Residual Randomization
Permutation procedure: Randomization of null model residuals
Number of permutations: 10000
Estimation method: Ordinary Least Squares
Sums of Squares and Cross-products: Type III
Effect sizes (Z) based on F distributions

                   Df      SS        MS      Rsq       F       Z Pr(>F)
linetype            1 0.00790 0.0078957 0.017428 14.7320  3.6016 0.0001
sex                 1 0.01081 0.0108102 0.023861 20.1698  4.4916 0.0001
centroid size       1 0.00437 0.0043681 0.009641  8.1500  2.7967 0.0017
linetype:sex        1 0.00011 0.0001087 0.000240  0.2027 -0.7990 0.7869
linetype:line       6 0.02960 0.0049331 0.065331  9.2043  6.2789 0.0001
linetype:sex:line   6 0.00525 0.0008746 0.011582  1.6318  1.2968 0.0976
.
Residuals         173 0.09272 0.0005360 0.204657
Total             189 0.45306
---

Call: procD.lm(f1 = shape ~ linetype + sex + linetype * sex +
linetype/line +
    linetype/line * sex + size, iter = 9999, SS.type = "III",      data
= pca_gdf)
```

Table 4 — Shape ANOVA All Mice by LINE Both Sexes (No Covariate, with Length, with Centroid)

4A (4N)--HR No Covariate

```
Analysis of Variance, using Residual Randomization
Permutation procedure: Randomization of null model residuals
Number of permutations: 10000
Estimation method: Ordinary Least Squares
Sums of Squares and Cross-products: Type III
Effect sizes (Z) based on F distributions

          Df       SS        MS      Rsq       F      Z Pr(>F)
line       3 0.038411 0.0128038 0.141180 23.4018 6.6768 0.0001
sex        1 0.025766 0.0257656 0.094701 47.0922 6.0334 0.0001
line:sex   3 0.003251 0.0010836 0.011949  1.9806 1.3823 0.0860
Residuals 91 0.049789 0.0005471 0.182998
Total     98 0.272074
---

Call: procD.lm(f1 = shape ~ line + sex + line * sex, iter = 9999,
SS.type = "III",      data = pelvis_gdf_HR)
```

4B (5N) --C No Covariate

```
Analysis of Variance, using Residual Randomization
Permutation procedure: Randomization of null model residuals
Number of permutations: 10000
Estimation method: Ordinary Least Squares
Sums of Squares and Cross-products: Type III
Effect sizes (Z) based on F distributions

          Df       SS        MS      Rsq       F      Z Pr(>F)
line       3 0.004946 0.0016486 0.031343  2.8929 2.0424 0.0201
sex        1 0.023379 0.0233795 0.148164 41.0251 5.9995 0.0001
line:sex   3 0.001889 0.0006296 0.011971  1.1049 0.3802 0.3542
Residuals 83 0.047300 0.0005699 0.299759
Total     90 0.157794
---

Call: procD.lm(f1 = shape ~ line + sex + line * sex, iter = 9999,
SS.type = "III",      data = pelvis_gdf_CTRL)
```

4C (4L) --HR Length

```
Analysis of Variance, using Residual Randomization
Permutation procedure: Randomization of null model residuals
Number of permutations: 10000
Estimation method: Ordinary Least Squares
Sums of Squares and Cross-products: Type III
Effect sizes (Z) based on F distributions

          Df       SS        MS      Rsq       F       Z Pr(>F)
line       3 0.037649 0.0125498 0.138379 22.7225  6.6474 0.0001
sex        1 0.023528 0.0235277 0.086475 42.5990  5.9131 0.0001
length     1 0.000081 0.0000813 0.000299  0.1472 -1.0266 0.8441
line:sex   3 0.003240 0.0010799 0.011907  1.9553  1.3618 0.0892
Residuals 90 0.049708 0.0005523 0.182699
Total     98 0.272074
---

Call: procD.lm(f1 = shape ~ line + sex + line * sex + length, iter =
9999,
    SS.type = "III", data = pelvis_gdf_HR)
```

4D (5L) --C Length

```
Analysis of Variance, using Residual Randomization
Permutation procedure: Randomization of null model residuals
Number of permutations: 10000
Estimation method: Ordinary Least Squares
Sums of Squares and Cross-products: Type III
Effect sizes (Z) based on F distributions

          Df       SS        MS      Rsq       F      Z Pr(>F)
line       3 0.004595 0.0015317 0.029121  2.6849 1.8912 0.0287
sex        1 0.022208 0.0222084 0.140743 38.9280 5.9691 0.0001
length     1 0.000519 0.0005193 0.003291  0.9103 0.3458 0.3671
line:sex   3 0.001702 0.0005672 0.010783  0.9942 0.2247 0.4102
Residuals 82 0.046781 0.0005705 0.296468
Total     90 0.157794
---

Call: procD.lm(f1 = shape ~ line + sex + line * sex + length, iter =
9999,
    SS.type = "III", data = pelvis_gdf_CTRL)
```

4E (4S) -- HR Centroid

```
Analysis of Variance, using Residual Randomization
Permutation procedure: Randomization of null model residuals
Number of permutations: 10000
Estimation method: Ordinary Least Squares
Sums of Squares and Cross-products: Type III
Effect sizes (Z) based on F distributions

          Df       SS        MS      Rsq       F      Z Pr(>F)
line       3 0.021289 0.0070963 0.078247 13.5177 5.8628 0.0001
sex        1 0.008242 0.0082419 0.030293 15.7001 4.0544 0.0001
size       1 0.002542 0.0025424 0.009344  4.8429 2.0633 0.0192
line:sex   3 0.003199 0.0010665 0.011759  2.0315 1.4418 0.0765
Residuals 90 0.047246 0.0005250 0.173653
Total     98 0.272074
---

Call: procD.lm(f1 = shape ~ line + sex + line * sex + size, iter =
9999,
    SS.type = "III", data = pelvis_gdf_HR)
```

4F (5S)--C Centroid

```
Analysis of Variance, using Residual Randomization
Permutation procedure: Randomization of null model residuals
Number of permutations: 10000
Estimation method: Ordinary Least Squares
Sums of Squares and Cross-products: Type III
Effect sizes (Z) based on F distributions

          Df       SS        MS      Rsq       F      Z Pr(>F)
line       3 0.003977 0.0013256 0.025203  2.4055 1.7089 0.0442
sex        1 0.006715 0.0067153 0.042557 12.1860 3.6222 0.0002
size       1 0.002113 0.0021127 0.013389  3.8339 1.7925 0.0363
line:sex   3 0.002130 0.0007099 0.013498  1.2883 0.6272 0.2700
Residuals 82 0.045188 0.0005511 0.286370
Total     90 0.157794
---

Call: procD.lm(f1 = shape ~ line + sex + line * sex + size, iter =
9999,
    SS.type = "III", data = pelvis_gdf_CTRL)
```

Table 5— Shape ANOVA FEMALE No Covariate, with Length, with Centroid

Table 5A (2N) — Shape ANOVA FEMALE No Covariate

```
Analysis of Variance, using Residual Randomization
Permutation procedure: Randomization of null model residuals
Number of permutations: 10000
Estimation method: Ordinary Least Squares
Sums of Squares and Cross-products: Type III
Effect sizes (Z) based on F distributions

              Df       SS        MS     Rsq      F      Z Pr(>F)
linetype       1 0.017874 0.0178744 0.14927 24.882 4.4325  1e-04
linetype:line  6 0.043357 0.0072262 0.36209 10.059 6.2400  1e-04
Residuals     84 0.060343 0.0007184 0.50394
Total         91 0.119742
---

Call: procD.lm(f1 = shape ~ linetype + linetype/line, iter = 9999,
SS.type = "III", data = pelvis_gdf_female)
```

Table 5B (2L)— Shape ANOVA FEMALE with LENGTH

```
Analysis of Variance, using Residual Randomization
Permutation procedure: Randomization of null model residuals
Number of permutations: 10000
Estimation method: Ordinary Least Squares
Sums of Squares and Cross-products: Type III
Effect sizes (Z) based on F distributions

              Df       SS        MS     Rsq       F       Z Pr(>F)
linetype       1 0.017206 0.0172056 0.14369 23.7198  4.4353 0.0001
length         1 0.000137 0.0001371 0.00115  0.1891 -0.8932 0.8103
linetype:line  6 0.041501 0.0069168 0.34658  9.5355  6.1174 0.0001
Residuals     83 0.060206 0.0007254 0.50279
Total         91 0.119742
---

Call: procD.lm(f1 = shape ~ linetype + linetype/line + length, iter =
9999,
    SS.type = "III", data = pelvis_gdf_female)
```

Table 5C (2S)— Shape ANOVA FEMALE with CENTROID SIZE

```
Analysis of Variance, using Residual Randomization
Permutation procedure: Randomization of null model residuals
Number of permutations: 10000
Estimation method: Ordinary Least Squares
Sums of Squares and Cross-products: Type III
Effect sizes (Z) based on F distributions

              Df       SS        MS     Rsq      F      Z Pr(>F)
linetype       1 0.004181 0.0041810 0.03492 6.2591 2.5132 0.0052
size           1 0.004899 0.0048990 0.04091 7.3338 2.6608 0.0026
linetype:line  6 0.027485 0.0045808 0.22953 6.8576 5.4434 0.0001
Residuals     83 0.055444 0.0006680 0.46303
Total         91 0.119742
---

Call: procD.lm(f1 = shape ~ linetype + linetype/line + size, iter =
9999,
    SS.type = "III", data = pelvis_gdf_female)
```

Table 6— Shape ANOVA MALE (No covariate, with Length, with Centroid)

Table 6A (3N) — Shape ANOVA MALE No Covariate

```
Analysis of Variance, using Residual Randomization
Permutation procedure: Randomization of null model residuals
Number of permutations: 10000
Estimation method: Ordinary Least Squares
Sums of Squares and Cross-products: Type III
Effect sizes (Z) based on F distributions

              Df       SS        MS     Rsq      F      Z Pr(>F)
linetype       1 0.017714 0.0177142 0.15580 43.386 4.5787  1e-04
linetype:line  6 0.068760 0.0114601 0.60477 28.068 8.8036  1e-04
Residuals     90 0.036746 0.0004083 0.32320
Total         97 0.113696
---

Call: procD.lm(f1 = shape ~ linetype + linetype/line, iter = 9999,
SS.type = "III", data = pelvis_gdf_male)
```

Table 6B (3L)— Shape ANOVA MALE with LENGTH as Covariate

```
Analysis of Variance, using Residual Randomization
Permutation procedure: Randomization of null model residuals
Number of permutations: 10000
Estimation method: Ordinary Least Squares
Sums of Squares and Cross-products: Type III
Effect sizes (Z) based on F distributions

              Df       SS        MS     Rsq       F       Z Pr(>F)
linetype       1 0.016918 0.0169182 0.14880 41.1517  4.5748 0.0001
length         1 0.000157 0.0001567 0.00138  0.3812 -0.2933 0.6135
linetype:line  6 0.067111 0.0111851 0.59026 27.2065  8.6200 0.0001
Residuals     89 0.036590 0.0004111 0.32182
Total         97 0.113696
---

Call: procD.lm(f1 = shape ~ linetype + linetype/line + length, iter =
9999,
    SS.type = "III", data = pelvis_gdf_male)
```

Table 6C (3S)— Shape ANOVA MALE with CENTROID SIZE as Covariate

```
Analysis of Variance, using Residual Randomization
Permutation procedure: Randomization of null model residuals
Number of permutations: 10000
Estimation method: Ordinary Least Squares
Sums of Squares and Cross-products: Type III
Effect sizes (Z) based on F distributions

              Df       SS        MS     Rsq       F      Z Pr(>F)
linetype       1 0.006707 0.0067068 0.05899 16.5395 3.4011 0.0001
size           1 0.000656 0.0006564 0.00577  1.6187 0.8664 0.2012
linetype:line  6 0.057964 0.0096607 0.50982 23.8240 8.6567 0.0001
Residuals     89 0.036090 0.0004055 0.31742
Total         97 0.113696
---

Call: procD.lm(f1 = shape ~ linetype + linetype/line + size, iter =
9999,
    SS.type = "III", data = pelvis_gdf_male)
```

Table 7— Shape ANOVA FEMALE HR LINES (No Covariate, with Length, with Centroid)

Table 7A (6N) — Shape ANOVA Female HR Lines No Covariate

```
Analysis of Variance, using Residual Randomization
Permutation procedure: Randomization of null model residuals
Number of permutations: 10000
Estimation method: Ordinary Least Squares
Sums of Squares and Cross-products: Type III
Effect sizes (Z) based on F distributions

          Df       SS        MS     Rsq      F      Z Pr(>F)
line       3 0.038411 0.0128038 0.51425 15.175 5.0842  1e-04
Residuals 43 0.036282 0.0008438 0.48575
Total     46 0.074693
---

Call: procD.lm(f1 = shape ~ line, iter = 9999, SS.type = "III", data =
pelvis_gdf_female_HR)
```

Table 7B (6L)— Shape ANOVA Female HR Lines Length

```
Analysis of Variance, using Residual Randomization
Permutation procedure: Randomization of null model residuals
Number of permutations: 10000
Estimation method: Ordinary Least Squares
Sums of Squares and Cross-products: Type III
Effect sizes (Z) based on F distributions

          Df       SS        MS     Rsq       F       Z Pr(>F)
line       3 0.038378 0.0127927 0.51381 15.0105  5.0742 0.0001
length     1 0.000487 0.0004874 0.00653  0.5719 -0.0417 0.5198
Residuals 42 0.035795 0.0008523 0.47922
Total     46 0.074693
---

Call: procD.lm(f1 = shape ~ line + length, iter = 9999, SS.type =
"III",
    data = pelvis_gdf_female_HR)
```

Table 7C (6S)— Shape ANOVA Female HR Lines Centroid Size

```
Analysis of Variance, using Residual Randomization
Permutation procedure: Randomization of null model residuals
Number of permutations: 10000
Estimation method: Ordinary Least Squares
Sums of Squares and Cross-products: Type III
Effect sizes (Z) based on F distributions

          Df       SS        MS     Rsq      F      Z Pr(>F)
line       3 0.018673 0.0062243 0.24999 7.8545 3.9861 0.0001
size       1 0.003000 0.0029995 0.04016 3.7852 1.7156 0.0426 *
Residuals 42 0.033282 0.0007924 0.44559
Total     46 0.074693
---

Call: procD.lm(f1 = shape ~ line + size, iter = 9999, SS.type = "III",
    data = pelvis_gdf_female_HR)
```

Table 8— Shape ANOVA FEMALE C LINES (no covariate, with length, with Centroid)

Table 8A (8N) — Shape ANOVA Female C Lines No Covariate

```
Analysis of Variance, using Residual Randomization
Permutation procedure: Randomization of null model residuals
Number of permutations: 10000
Estimation method: Ordinary Least Squares
Sums of Squares and Cross-products: Type III
Effect sizes (Z) based on F distributions

          Df         SS          MS     Rsq      F      Z Pr(>F)
line       3 0.0049458 0.00164860 0.17051 2.8092 2.0272 0.0205
Residuals 41 0.0240608 0.00058685 0.82949
Total     44 0.0290066
---

Call: procD.lm(f1 = shape ~ line, iter = 9999, SS.type = "III", data =
pelvis_gdf_female_CTRL)
```

Table 8B (8L) — Shape ANOVA Female C Lines Length

```
Analysis of Variance, using Residual Randomization
Permutation procedure: Randomization of null model residuals
Number of permutations: 10000
Estimation method: Ordinary Least Squares
Sums of Squares and Cross-products: Type III
Effect sizes (Z) based on F distributions

          Df         SS          MS     Rsq      F       Z Pr(>F)
line       3 0.0041954 0.00139847 0.14464 2.4278 1.74011 0.0405
length     1 0.0010200 0.00102002 0.03517 1.7708 0.93722 0.1767
Residuals 40 0.0230408 0.00057602 0.79433
Total     44 0.0290066
---

Call: procD.lm(f1 = shape ~ line + length, iter = 9999, SS.type =
"III",
    data = pelvis_gdf_female_CTRL)
```

Table 8C (8S) —Shape ANOVA Female C Lines Centroid Size

```
Analysis of Variance, using Residual Randomization
Permutation procedure: Randomization of null model residuals
Number of permutations: 10000
Estimation method: Ordinary Least Squares
Sums of Squares and Cross-products: Type III
Effect sizes (Z) based on F distributions

          Df        SS         MS     Rsq      F      Z Pr(>F)
line       3 0.0044969 0.00149898 0.15503 2.8503 2.1158 0.0176
size       1 0.0030243 0.00302435 0.10426 5.7507 2.3667 0.0076
Residuals 40 0.0210365 0.00052591 0.72523
Total     44 0.0290066
---

Call: procD.lm(f1 = shape ~ line + size, iter = 9999, SS.type = "III",
    data = pelvis_gdf_female_CTRL)
```

Table 9— Shape ANOVA MALE HR LINES (No Covariate, with Length, with Centroid)

Table 9A (7N) — Shape ANOVA Male HR Lines No Covariate

```
Analysis of Variance, using Residual Randomization
Permutation procedure: Randomization of null model residuals
Number of permutations: 10000
Estimation method: Ordinary Least Squares
Sums of Squares and Cross-products: Type III
Effect sizes (Z) based on F distributions

          Df       SS        MS     Rsq      F      Z Pr(>F)
line       3 0.062983 0.0209944 0.82342 74.609 9.0215  1e-04
Residuals 48 0.013507 0.0002814 0.17658
Total     51 0.076490
---

Call: procD.lm(f1 = shape ~ line, iter = 9999, SS.type = "III", data =
pelvis_gdf_male_HR)
```

Table 9B (7L) — Shape ANOVA Male HR Lines length

```
Analysis of Variance, using Residual Randomization
Permutation procedure: Randomization of null model residuals
Number of permutations: 10000
Estimation method: Ordinary Least Squares
Sums of Squares and Cross-products: Type III
Effect sizes (Z) based on F distributions

          Df       SS        MS     Rsq      F      Z Pr(>F)
line       3 0.060256 0.0200853 0.78776 71.937 8.9609 0.0001
length     1 0.000384 0.0003842 0.00502  1.376 0.6665 0.2583
Residuals 47 0.013123 0.0002792 0.17156
Total     51 0.076490
---

Call: procD.lm(f1 = shape ~ line + length, iter = 9999, SS.type =
"III",
    data = pelvis_gdf_male_HR)
```

Table 9C (7S)— Shape ANOVA Male HR Lines Centroid Size

```
Analysis of Variance, using Residual Randomization
Permutation procedure: Randomization of null model residuals
Number of permutations: 10000
Estimation method: Ordinary Least Squares
Sums of Squares and Cross-products: Type III
Effect sizes (Z) based on F distributions

          Df       SS        MS     Rsq       F      Z Pr(>F)
line       3 0.046701 0.0155669 0.61054 56.4176 8.6809 0.0001
size       1 0.000538 0.0005385 0.00704  1.9516 1.0386 0.1514
Residuals 47 0.012968 0.0002759 0.16954
Total     51 0.076490
---

Call: procD.lm(f1 = shape ~ line + size, iter = 9999, SS.type = "III",
    data = pelvis_gdf_male_HR)
```

Table 10— Shape ANOVA Male C Lines (No Covariate, with Length, with Centroid)

Table 10A (9N)— Shape ANOVA Male C Lines No Covariate

```
Analysis of Variance, using Residual Randomization
Permutation procedure: Randomization of null model residuals
Number of permutations: 10000
Estimation method: Ordinary Least Squares
Sums of Squares and Cross-products: Type III
Effect sizes (Z) based on F distributions

          Df        SS         MS    Rsq      F      Z Pr(>F)
line       3 0.0057771 0.00192569 0.1991 3.4802 2.0624  0.0180
Residuals 42 0.0232394 0.00055332 0.8009
Total     45 0.0290165
---

Call: procD.lm(f1 = shape ~ line, iter = 9999, SS.type = "III", data =
pelvis_gdf_male_CTRL)
```

Table 10B (9L) — Shape ANOVA Male C Lines Length

```
Analysis of Variance, using Residual Randomization
Permutation procedure: Randomization of null model residuals
Number of permutations: 10000
Estimation method: Ordinary Least Squares
Sums of Squares and Cross-products: Type III
Effect sizes (Z) based on F distributions

          Df        SS         MS     Rsq      F        Z Pr(>F)
line       3 0.0059088 0.00196960 0.20364 3.5087  2.07583  0.0170
length     1 0.0002240 0.00022404 0.00772 0.3991 -0.14874  0.5540
Residuals 41 0.0230154 0.00056135 0.79318
Total     45 0.0290165
---

Call: procD.lm(f1 = shape ~ line + length, iter = 9999, SS.type =
"III",
    data = pelvis_gdf_male_CTRL)
```

Table 10C (9S)— Shape ANOVA Male C Lines Centroid Size

```
Analysis of Variance, using Residual Randomization
Permutation procedure: Randomization of null model residuals
Number of permutations: 10000
Estimation method: Ordinary Least Squares
Sums of Squares and Cross-products: Type III
Effect sizes (Z) based on F distributions

          Df        SS         MS     Rsq      F        Z Pr(>F)
line       3 0.0052992 0.00176641 0.18263 3.1494  1.88803 0.0280
size       1 0.0002439 0.00024388 0.00840 0.4348 -0.09334 0.5358
Residuals 41 0.0229956 0.00056087 0.79250
Total     45 0.0290165
---

Call: procD.lm(f1 = shape ~ line + size, iter = 9999, SS.type = "III",
    data = pelvis_gdf_male_CTRL)
```

Figures

Figure 1. Whole-Body Scan of Same Mouse (ID 96186)

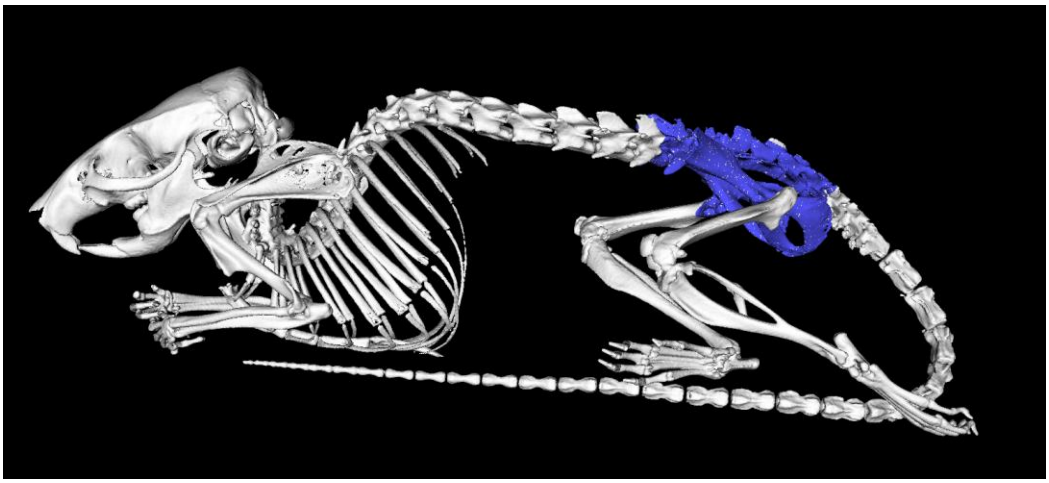

Lateral view

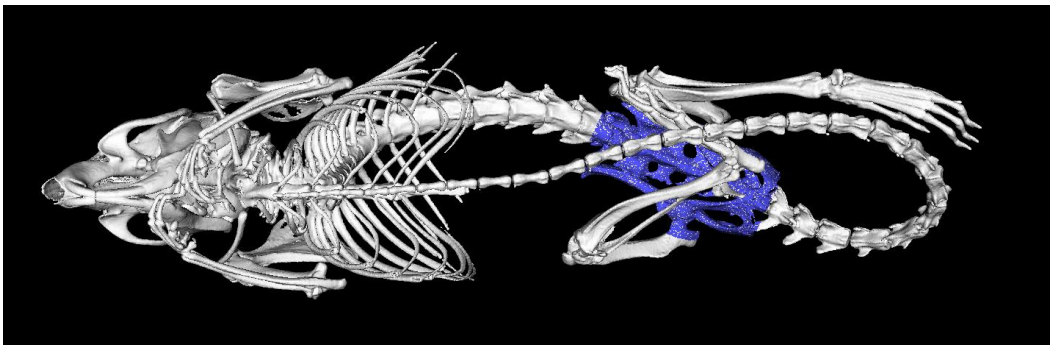

Ventral view

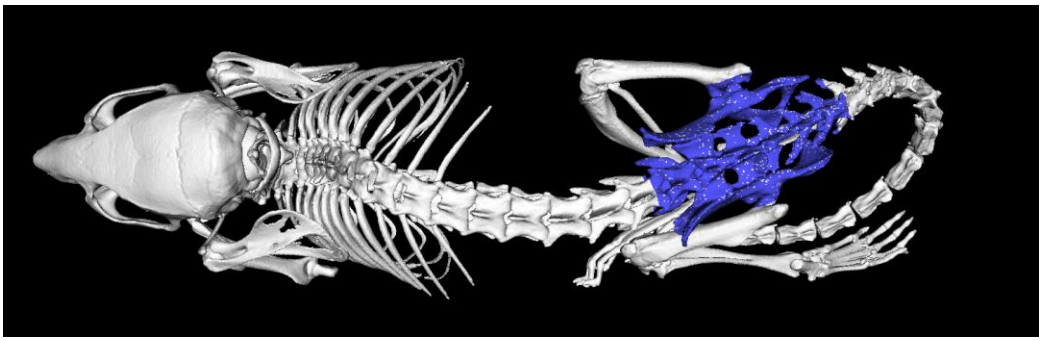

Dorsal View

MouseID: 96186

Figure 1. Whole-Body Scan of Same Mouse (ID 96186)

Three-dimensional micro-computed tomography (micro-CT) reconstruction of a representative mouse skeleton. The pelvic girdle is highlighted in purple and shown in lateral (top), ventral (middle), and dorsal (bottom) views. These views illustrate the anatomical region used for geometric morphometric landmark placement and shape analyses.

Figure 2. 44 Landmarks in Methods (ID 96186)

A)

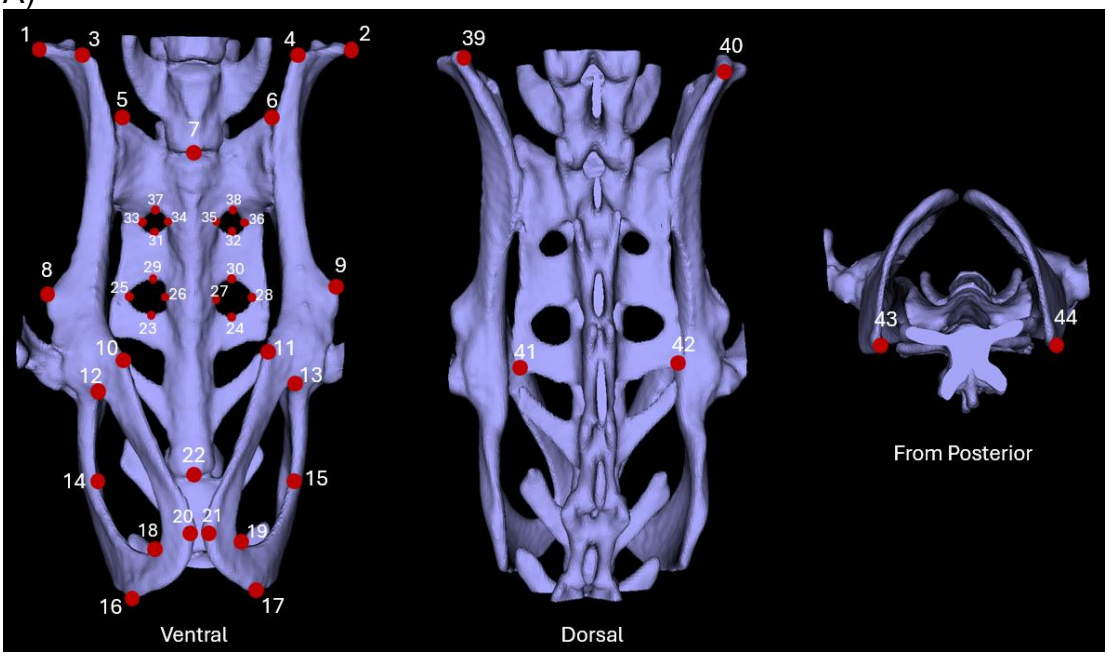

MouseID: 96186

B) Labeled pelvis bones

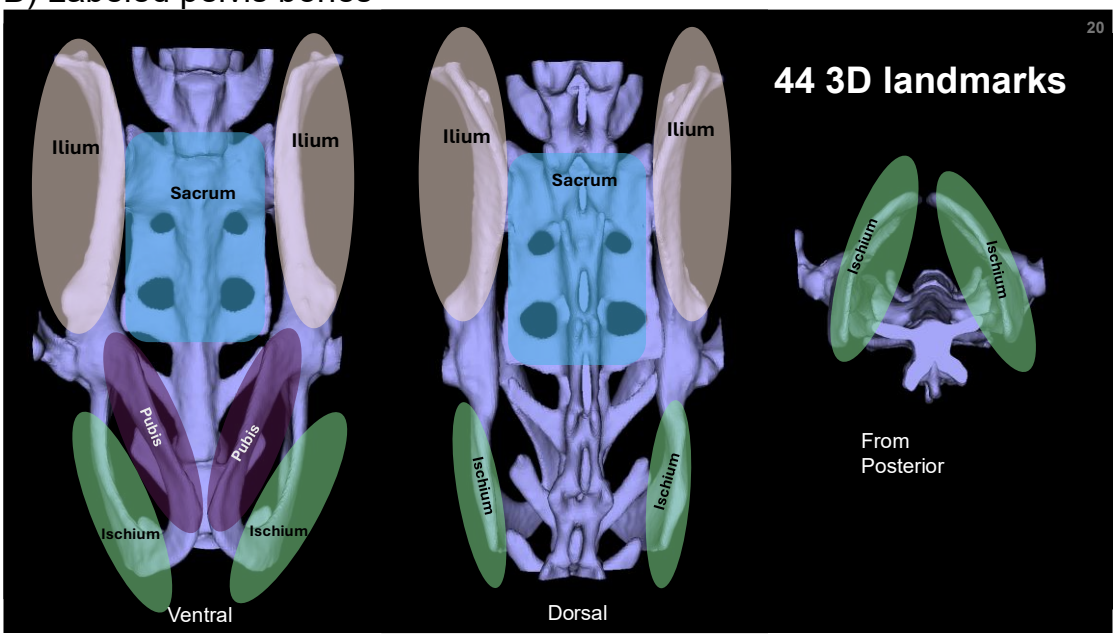

Figure 2. 44 Landmarks in Methods (ID 96186)

A) Isolated three-dimensional micro-computed tomography (micro-CT) reconstruction of the pelvis girdle. Angles shown in lateral (top), ventral (middle), and dorsal (bottom) views. The red dot indicate the 44 landmarks placed around the pelvic region used for geometric morphometric landmark placement and shape analyses. B) Labeled pelvis bones: Ilium, ischium, and pubis.

Figure 3 A) Body Length & B) Centroid Size 2 Panels by Line and Sex from SAS

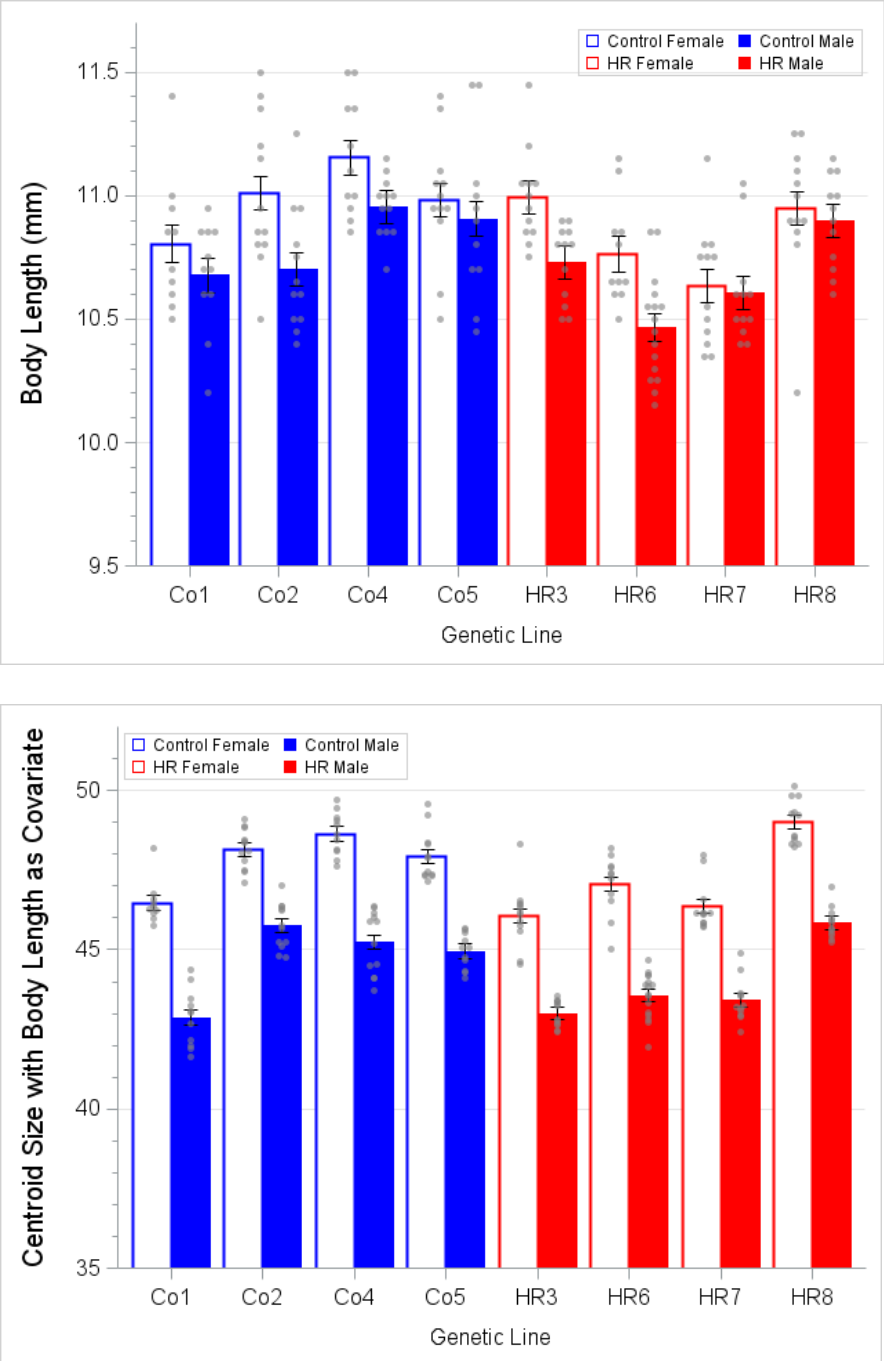

Figure 3 A) Body Length & B) Centroid Size 2 Panels by Line and Sex from SAS

A) Body length (mm) (tip of nose to base of tail) of mice for the 4 non-selected Control (Co1, Co2, Co4, Co5) and 4 selectively bred High Runner (HR3, HR6, HR7, HR8) genetic lines, separated by sex. White bars represent females and colored bars represent males. Blue indicates Control lines and red indicates High Runner lines. Values are least squares means ± SEM from SAS Procedure Mixed (see Methods), and gray points represent individual mice (residuals + LSM for their subgroup).
B) Pelvis centroid size, adjusted for body length as a covariate.

Figure 4 A) PC1 vs PC2 Both Sexes; B) X, Y TPS Grid PC1 and PC2

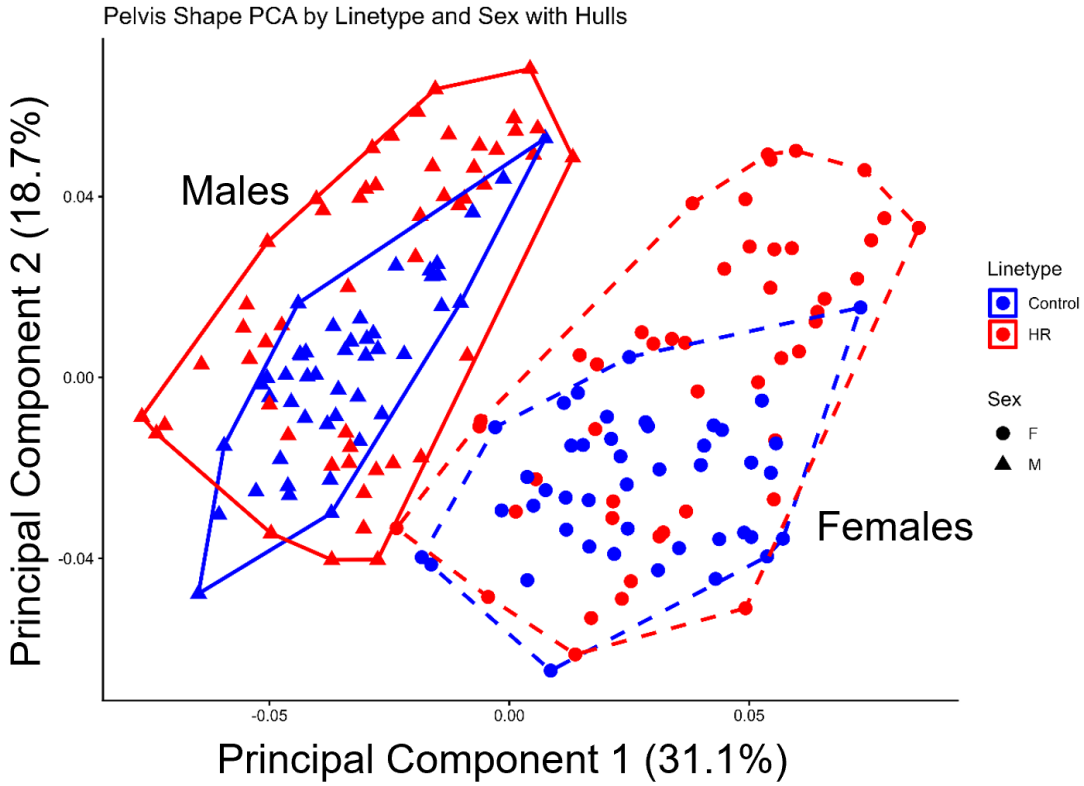

Figure 4 continued

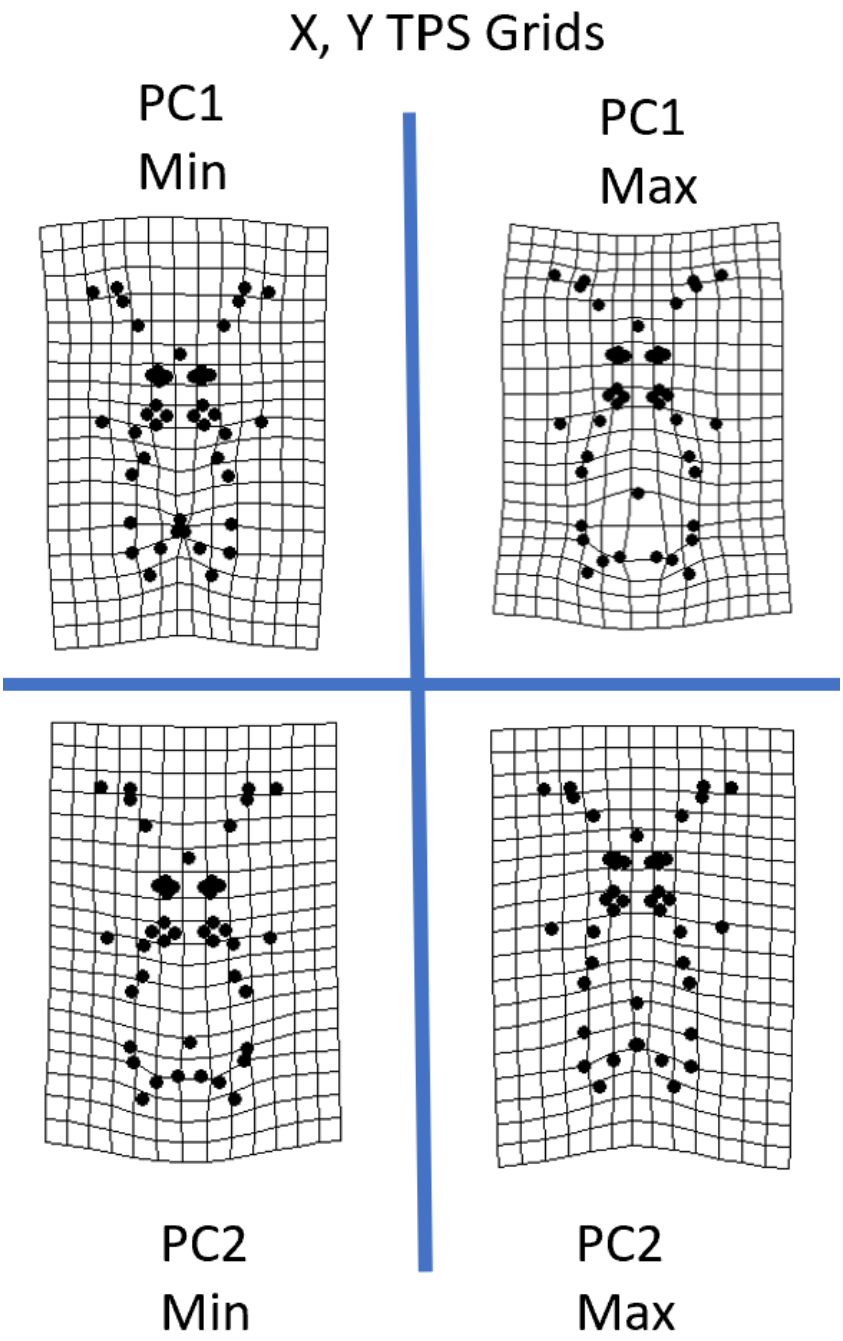

Figure 4 A) PC1 vs PC2 Both Sexes; B) X, Y TPS Grid PC1 and PC2

A) Principal component analysis (PCA) of pelvis shape based on Procrustes-aligned landmark coordinates. X-axis has PCA 1 and y-axis has PCA 2. Each point represents an individual mouse (N=190 specimens). Colors indicate linetype (blue = Control, red = High Runner), and symbols indicate sex (circles = females, triangles = males). Convex hulls outline the distribution of specimens within each linetype-sex group, illustrating the range of shape variation along the first two principal components. B) X,Y TPS Grid for PC1 and PC2 minimum and maximum points.

Figure 5 A) PC3 vs PC4 Both Sexes; B) X, Y TPS Grid PC3 and PC4

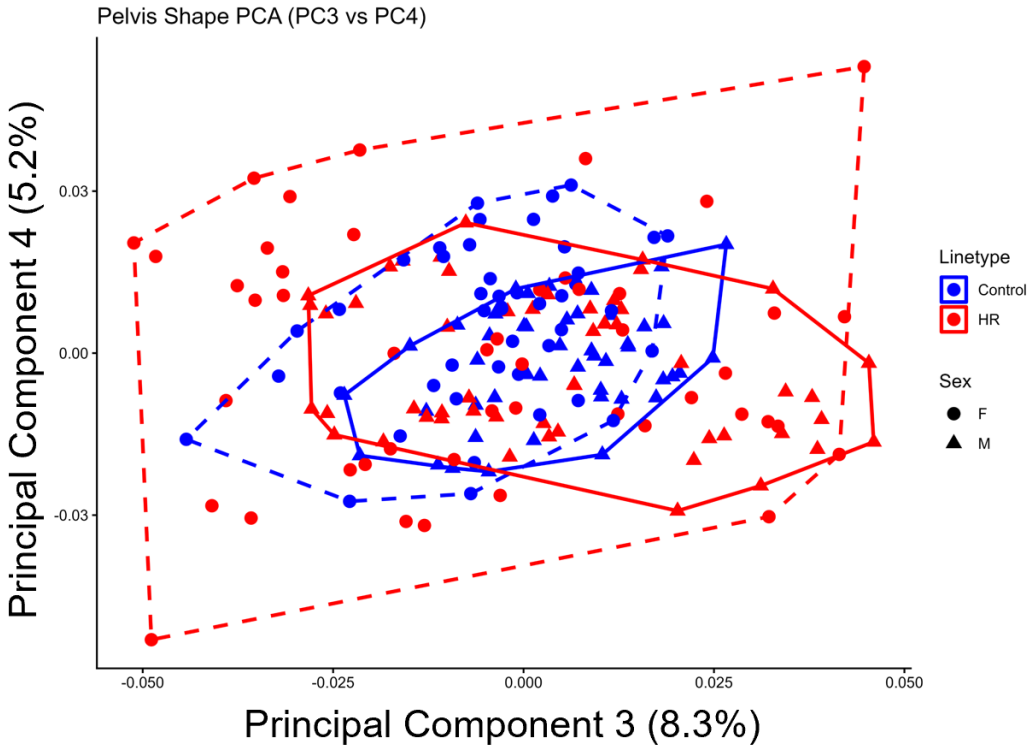

Figure 5 continued

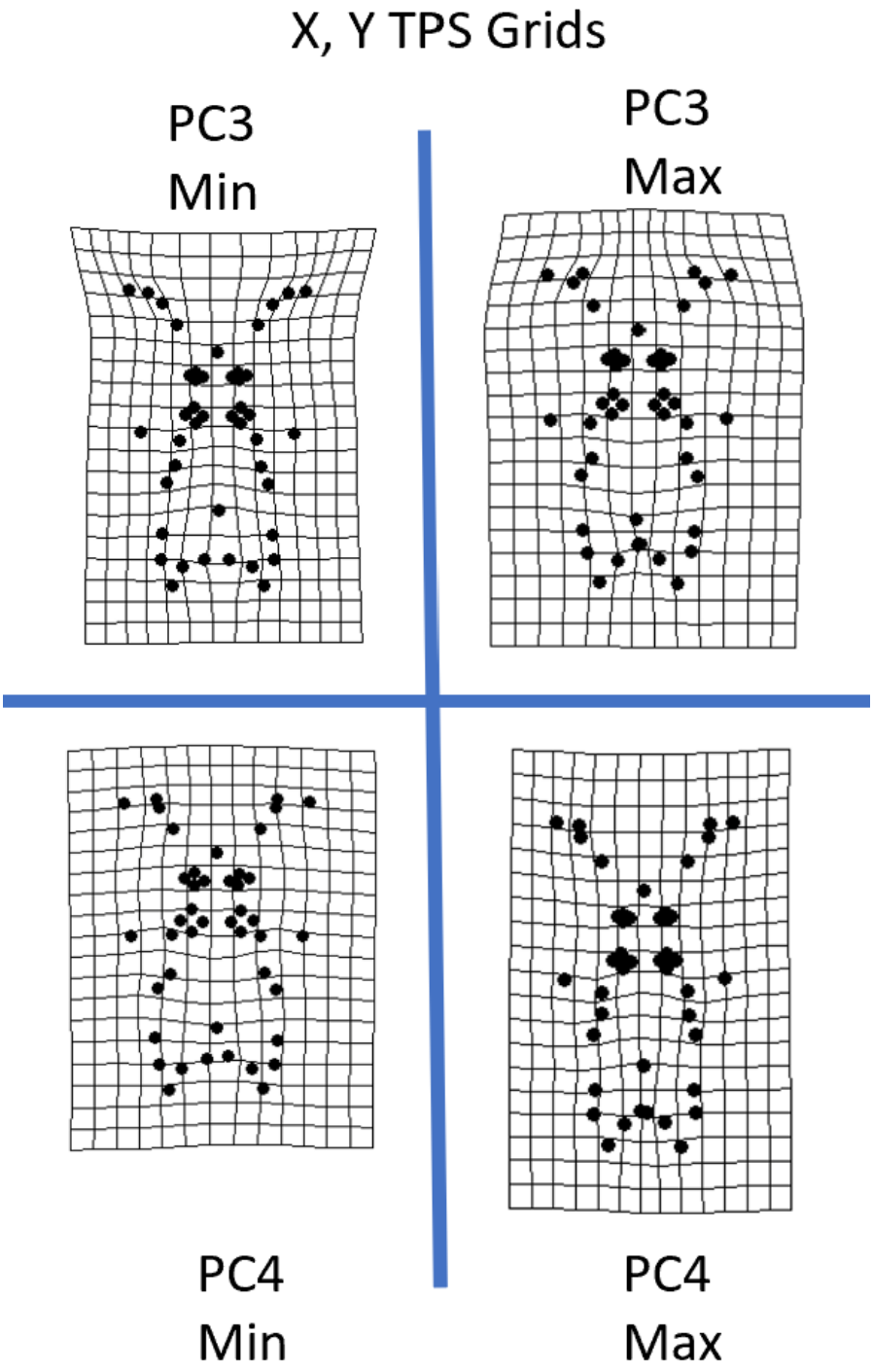

Figure 5 A) PC3 vs PC4 Both Sexes; B) X, Y TPS Grid PC3 and PC4

A) Principal component analysis (PCA) of pelvis shape showing variation along Principal Components 3 and 4 based on Procrustes-aligned landmark coordinates. X-axis has PCA 3 and y-axis has PCA 4. Each point represents an individual mouse. Colors indicate linetype (blue = Control, red = High Runner), and symbols indicate sex (circles = females, triangles = males). Convex hulls outline the distribution of specimens within each linetype–sex group, illustrating the extent of within-group shape variation and overlap along PC3 and PC4. B) X,Y TPS Grid for PC3 and PC4 minimum and maximum points.

Figure 6 PC1 vs PC2 by Line Females and Then Males

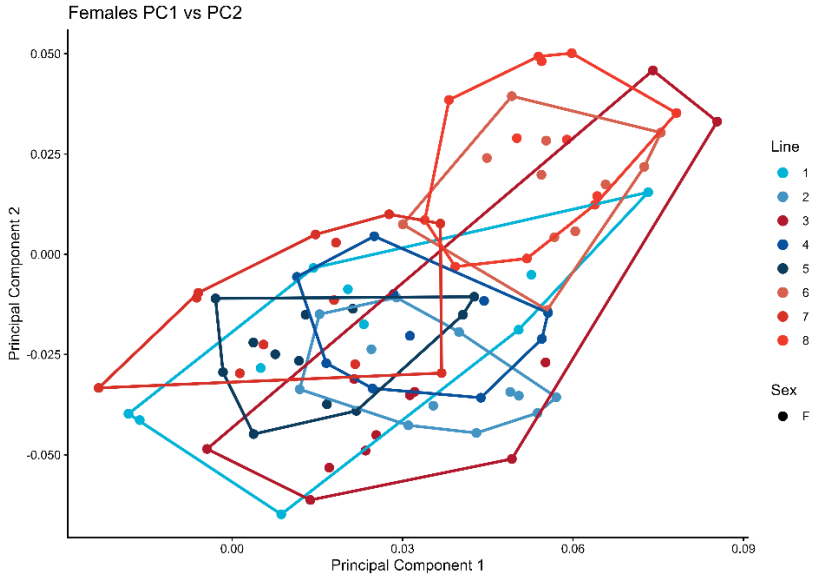

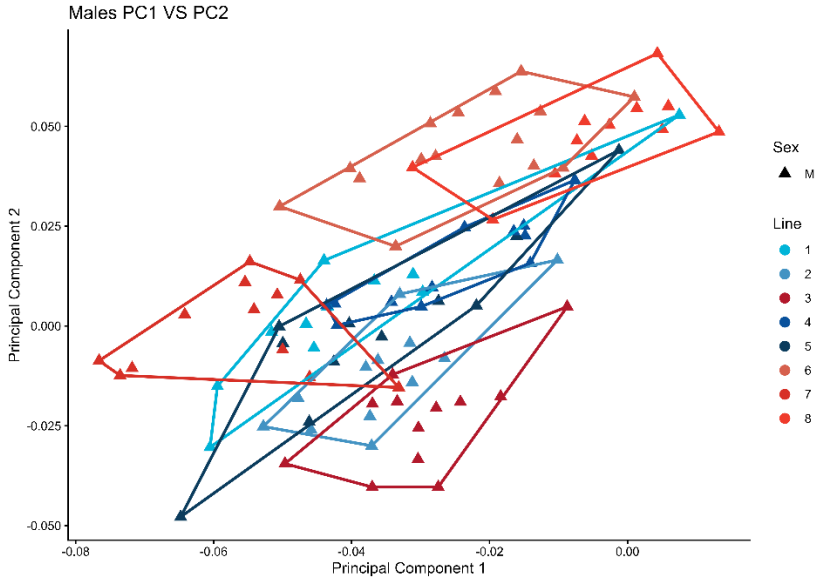

Figure 6 PC1 vs PC2 by Line Females and Then Males

Female only portion of the Principal Component Analysis (PCA) 1 and 2 of pelvis shape based on Procrustes-aligned landmark coordinates. X-axis has PCA 1 and y-axis has PCA 2. Each point represents an individual female mouse (N=92 specimens). Colors indicate each of the 8 lines (Control lines are in blue shades and HR lines are in red shades). Convex hulls outline the distribution of specimens within each line, illustrating the range of shape variation along the first two principal components.

Male only portion of the Principal Component Analysis (PCA) 1 and 2 of pelvis shape based on Procrustes-aligned landmark coordinates. X-axis has PCA 1 and y-axis has PCA 2. Each point represents an individual female mouse (N=98 specimens). Colors indicate each of the 8 lines (Control lines are in blue shades and HR lines are in red shades). Convex hulls outline the distribution of specimens within each line, illustrating the range of shape variation along the first two principal components.

Figure 7 PC3 vs PC4 by Line Females and Then Males

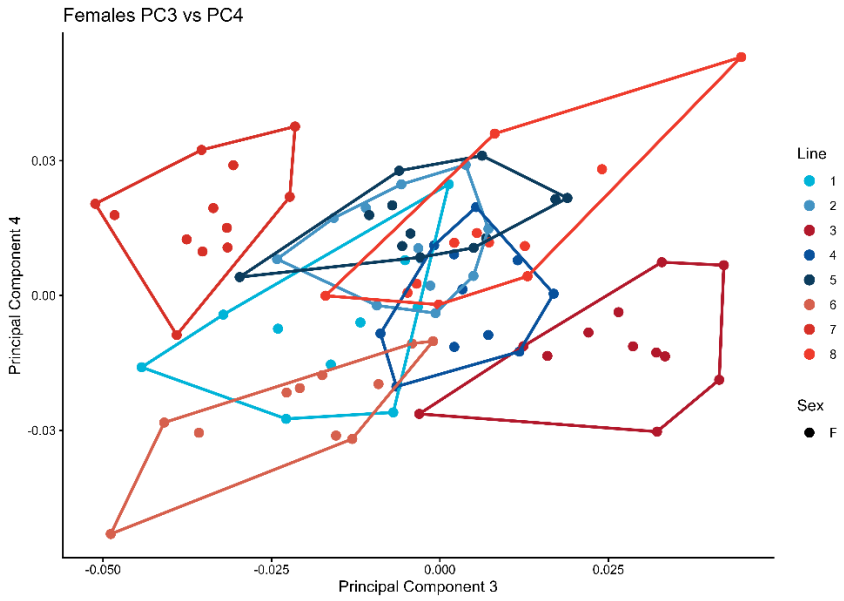

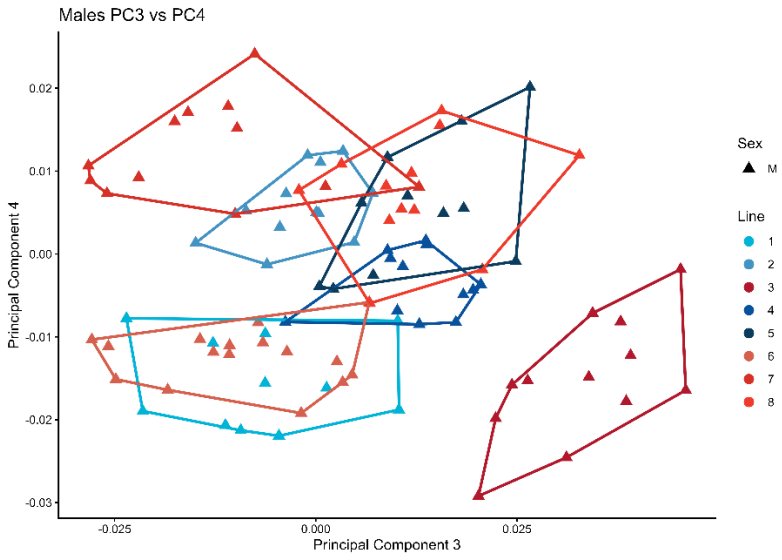

Figure 7 PC3 vs PC4 by Line Females and Then Males

Female only portion of the Principal Component Analysis (PCA) 3 and 4 of pelvis shape based on Procrustes-aligned landmark coordinates. X-axis has PCA 3 and y-axis has PCA 4. Each point represents an individual female mouse (N=92 specimens). Colors indicate each of the 8 lines (Control lines are in blue shades and HR lines are in red shades). Convex hulls outline the distribution of specimens within each line, illustrating the range of shape variation along principal components 3 and 4.

Male only portion of the Principal Component Analysis (PCA) 3 and 4 of pelvis shape based on Procrustes-aligned landmark coordinates. X-axis has PCA 3 and y-axis has PCA 4. Each point represents an individual female mouse (N=98 specimens). Colors indicate each of the 8 lines (Control lines are in blue shades and HR lines are in red shades). Convex hulls outline the distribution of specimens within each line, illustrating the range of shape variation along principal components 3 and 4.

Figure 8 Morphological Disparity (all 125 PCAs)

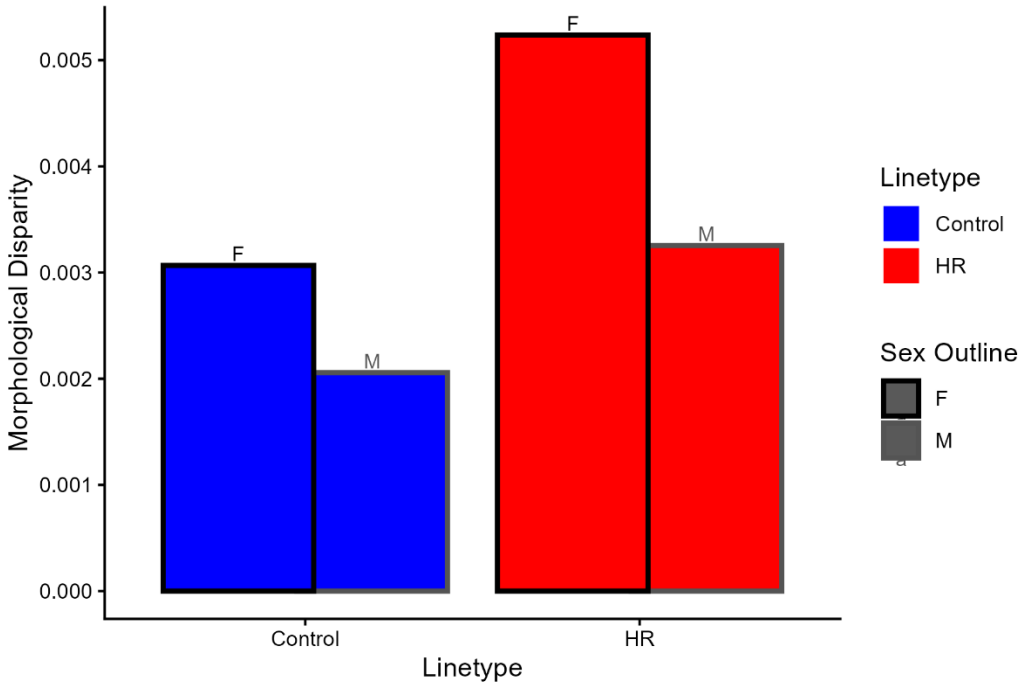

Figure 8 Morphological Disparity (all 125 PCAs)

Procrustes variance was calculated separately for Control and High Runner (HR) mice within each sex using morphological disparity analysis. Bars represent within-group Procrustes variance; black and gray outlines indicate females and males, respectively.

References Cited in Zotero

Alfaro, M. E., D. I. Bolnick, and P. C. Wainwright. 2004. Evolutionary dynamics of complex biomechanical systems: an example using the four-bar mechanism. Evolution 58:495–503.

Álvarez, A., M. D. Ercoli, and F. J. Prevosti. 2013. Locomotion in some small to medium-sized mammals: a geometric morphometric analysis of the penultimate lumbar vertebra, pelvis and hindlimbs. Zoology 116:356–371.

Baken, E. K., M. L. Collyer, A. Kaliontzopoulou, and D. C. Adams. 2021. geomorph v4.0 and gmShiny: Enhanced analytics and a new graphical interface for a comprehensive morphometric experience. Methods Ecol. Evol. 12:2355–2363.

Belyaev, R. I., G. G. Boeskorov, A. N. Kuznetsov, M. Rotonda, and N. E. Prilepskaya. 2025. Comparative study of the body proportions in Elephantidae and other large herbivorous mammals. J. Anat. 246:63–85.

Berdnikovs, S., M. Bernstein, A. Metzler, and R. Z. German. 2007. Pelvic growth: Ontogeny of size and shape sexual dimorphism in rat pelves. J. Morphol. 268:12–22.

Bernstein, P., and E. S. Crelin. 1967. Bony pelvic sexual dimorphism in the rat. Anat. Rec. 157:517–525.

Blomberg, S. P., and T. Garland, Jr. 2002. Tempo and mode in evolution: phylogenetic inertia, adaptation and comparative methods. J. Evol. Biol. 15:899–910.

Blomberg, S. P., T. Garland, Jr., and A. R. Ives. 2003. Testing for phylogenetic signal in comparative data: behavioral traits are more labile. Evolution 57:717–745.

Careau, V., M. E. Wolak, P. A. Carter, and T. Garland, Jr. 2013. Limits to behavioral evolution: the quantitative genetics of a complex trait under directional selection. Evolution 67:3102–3119.

Carrano, M. T. 1999. What, if anything, is a cursor? Categories versus continua for determining locomotor habit in mammals and dinosaurs. J. Zool. 247:29-42.

Castro, A. A., and T. Garland, Jr. 2018. Evolution of hindlimb bone dimensions and muscle masses in house mice selectively bred for high voluntary wheel-running behavior. J. Morphol. 279:766–779.

Castro, A. A., A. Nguyen, S. Ahmed, T. Garland, Jr., and N. C. Holt. 2024. Muscle-tendon unit properties in mice selected for high levels of voluntary running: novel physiologies, co-adaptation, trade-offs, and multiple solutions in the evolution of cursoriality. Ecol. Evol. Physiol. 97:191–208.

Castro, A. A., H. Rabitoy, G. C. Claghorn, and T. Garland, Jr. 2021. Rapid and longer-term effects of selective breeding for voluntary exercise behavior on skeletal morphology in house mice. J. Anat. 238:720–742.

Cignoni, P., M. Callieri, M. Corsini, M. Dellepiane, F. Ganovelli, and G. Ranzuglia. 2008. MeshLab: an open-source mesh processing tool. Pp. 129–136 *in* Eurographics Italian Chapter Conference. The Eurographics Association.

Copes, L. E., H. Schutz, E. M. Dlugosz, W. Acosta, M. A. Chappell, and T. Garland, Jr. 2015. Effects of voluntary exercise on spontaneous physical activity and food consumption in mice: results from an artificial selection experiment. Physiol. Behav. 149:86–94.

Csanády, A., P. Krišovský, and L. Hlôška. 2019. Pelvic and sacral size dimorphism and allometry in two predatory carnivores with different life histories and locomotory adaptations. Turk. J. Zool. 43:580–591.

Dalstra, M., and R. Huiskes. 1995. Load transfer across the pelvic bone. J. Biomech. 28:715–724.

Dlugosz, E. M., M. A. Chappell, D. G. McGillivray, D. A. Syme, and T. Garland, Jr. 2009. Locomotor trade-offs in mice selectively bred for high voluntary wheel running. J. Exp. Biol. 212:2612–2618.

Dunmire, W. W. 1955. Sex dimorphism in the pelvis of rodents. J. Mammal. 36:356–361.

Esteban, J. M., A. Martín-Serra, C. Varón-González, A. Pérez-Ramos, D. Velasco, F. J. Pastor, and B. Figueirido. 2020. Morphological evolution of the carnivoran sacrum. J. Anat. 237:1087–1102.

Gardner, W. U. 1936. Sexual dimorphism of the pelvis of the mouse, the effect of estrogenic hormones upon the pelvis and upon the development of scrotal hernias. Am. J. Anat. 59:459–483.

Garland, Jr., T. 2003. Selection experiments: an under-utilized tool in biomechanics and organismal biology. Pp. 23–56 *in* V. L. Bels, J.-P. Gasc, and A. Casinos, eds. Vertebrate biomechanics and evolution. BIOS Scientific Publishers Ltd., Oxford, U.K.

Garland, Jr., T., C. J. Downs, and A. R. Ives. 2022. Trade-Offs (and Constraints) in Organismal Biology. Physiol. Biochem. Zool. 95:82–112.

Garland, Jr., T., and P. W. Freeman. 2005. Selective breeding for high endurance running increases hindlimb symmetry. Evolution 59:1851–1854.

Garland, Jr., T., and C. M. Janis. 1993. Does metatarsal/femur ratio predict maximal running speed in cursorial mammals? J. Zool. 229:133–151.

Garland, Jr., T., S. A. Kelly, J. L. Malisch, E. M. Kolb, R. M. Hannon, B. K. Keeney, S. L. Van Cleave, and K. M. Middleton. 2011. How to run far: multiple solutions and sex-specific responses to selective breeding for high voluntary activity levels. Proc. R. Soc. B Biol. Sci. 278:574–581.

Garland, Jr., T., M. T. Morgan, J. G. Swallow, J. S. Rhodes, I. Girard, J. G. Belter, and P. A. Carter. 2002. Evolution of a small-muscle polymorphism in lines of house mice selected for high activity levels. Evolution 56:1267–1275.

Hillis, D. A., and T. Garland. 2023. Multiple solutions at the genomic level in response to selective breeding for high locomotor activity. GENETICS 223:iyac165.

Hiramatsu, L., and T. Garland, Jr. 2018. Mice selectively bred for high voluntary wheel-running behavior conserve more fat despite increased exercise. Physiol. Behav. 194:1–8.

Hogervorst, T., H. W. Bouma, and J. de Vos. 2009. Evolution of the hip and pelvis. Acta Orthop. 80:1–39.

Kazhdan, M., and H. Hoppe. 2013. Screened poisson surface reconstruction. ACM Trans Graph 32:29:1-29:13.

Kelly, S. A., P. P. Czech, J. T. Wight, K. M. Blank, and T. Garland, Jr. 2006. Experimental evolution and phenotypic plasticity of hindlimb bones in high-activity house mice. J. Morphol. 267:360–374.

Khan, R. H., J. S. Rhodes, I. A. Girard, N. E. Schwartz, and T. Garland, Jr. 2024. Does behavior evolve first? Correlated responses to selection for voluntary wheel-running behavior in house mice. Ecol. Evol. Physiol. 97:97–117.

Kikinis, R., S. D. Pieper, and K. G. Vosburgh. 2014. 3D Slicer: A Platform for Subject-Specific Image Analysis, Visualization, and Clinical Support. Pp. 277–289 *in* F. A. Jolesz, ed. Intraoperative Imaging and Image-Guided Therapy. Springer, New York, NY.

Klingenberg, C. P. 2016. Size, shape, and form: concepts of allometry in geometric morphometrics. Dev. Genes Evol. 226:113–137.

Lewton, K. L. 2015. Pelvic form and locomotor adaptation in strepsirrhine primates. Anat. Rec. 298:230–248.

Lewton, K. L., R. Brankovic, W. A. Byrd, D. Cruz, J. Morales, and S. Shin. 2020. The effects of phylogeny, body size, and locomotor behavior on the three-dimensional shape of the pelvis in extant carnivorans. PeerJ 8:e8574.

Lewton, K. L., T. Ritzman, L. E. Copes, T. Garland, Jr., and T. D. Capellini. 2019. Exercise-induced loading increases ilium cortical area in a selectively-bred mouse model. Am. J. Phys. Anthropol. 168:543–551.

Lionberger, D., P. S. Walker, and J. Granholm. 1985. Effects of prosthetic acetabular replacement on strains in the pelvis. J. Orthop. Res. 3:372–379.

Malisch, J. L., C. W. Breuner, E. M. Kolb, H. Wada, R. M. Hannon, M. A. Chappell, K. M. Middleton, and T. Garland, Jr. 2009. Behavioral despair and home-cage activity in mice with chronically elevated baseline corticosterone concentrations. Behav. Genet. 39:192–201.

Martín-Serra, A., B. Figueirido, and P. Palmqvist. 2014. A three-dimensional analysis of the morphological evolution and locomotor behaviour of the carnivoran hind limb. BMC Evol. Biol. 14:129.

McPherson, F. J., and P. J. Chenoweth. 2012. Mammalian sexual dimorphism. Anim. Reprod. Sci. 131:109–122.

Meek, T. H., B. P. Lonquich, R. M. Hannon, and T. Garland, Jr. 2009. Endurance capacity of mice selectively bred for high voluntary wheel running. J. Exp. Biol. 212:2908–2917.

Moen, D. S. 2019. What determines the distinct morphology of species with a particular ecology? The roles of many-to-one mapping and trade-offs in the evolution of frog ecomorphology and performance. Am. Nat. 194:E81–E95.

Mpagike, F. H., and M. Makungu. 2024. Radiological anatomy of the pelvis and pelvic limb of the greater cane rat (*Thryonomys swinderianus*). Vet. Med. Int. 2024:5998717.

Pallandre, J.-P., F. Lavenne, E. Pellé, G. Breton, M. Ribaud, and V. Bels. 2021. Variation in the sacroiliac joint in Felidae. PeerJ 9:e11116.

Ricklan, S. J., S.-L. Decrausaz, J. C. K. Wells, and J. T. Stock. 2021. Obstetric dimensions of the female pelvis are less integrated than locomotor dimensions and show protective scaling patterns: Implications for the obstetrical dilemma. Am. J. Hum. Biol. 33:e23451.

Rohlf, F. J., and D. Slice. 1990. Extensions of the procrustes method for the optimal superimposition of landmarks. Syst. Zool. 39:40.

Rose, M. R., and T. Garland, Jr. 2009. Darwin’s other mistake.

Schutz, H., E. R. Donovan, and J. P. Hayes. 2009a. Effects of parity on pelvic size and shape dimorphism in *Mus*. J. Morphol. 270:834–842.

Schutz, H., P. D. Polly, J. D. Krieger, and R. P. Guralnick. 2009b. Differential sexual dimorphism: size and shape in the cranium and pelvis of grey foxes (*Urocyon*). Biol. J. Linn. Soc. 96:339–353.

Schwartz, N. E., M. P. McNamara, J. M. Orozco, J. O. Rashid, A. P. Thai, and T. Garland. 2023. Selective breeding for high voluntary exercise in

mice increases maximal ($\dot{V}O2,max$) but not basal metabolic rate. J. Exp. Biol. 226:jeb245256.

Schwartz, N., and T. Garland, Jr. 2024. A meta-analysis of whole-body and heart mass effect sizes from a long-term artificial selection experiment for high voluntary exercise. J. Exp. Biol. 227:jeb249213.

Sengupta, P. 2013. The laboratory rat: relating its age with human's. Int. J. Prev. Med. 4:624–630.

Siegel, M. I., and C. L. Jones. 1975. The skeletal correlates of behavioral modification in the laboratory mouse (Mus musculus). Am. J. Phys. Anthropol. 42:141–144.

Swallow, J. G., P. A. Carter, and T. Garland, Jr. 1998. Artificial selection for increased wheel-running behavior in house mice. Behav. Genet. 28:227–237.

Swallow, J. G., J. P. Hayes, P. Koteja, and T. Garland, Jr. 2009. Selection experiments and experimental evolution of performance and physiology. Pp. 301–351 *in* T. Garland, Jr. and M. R. Rose, eds. Experimental evolution: concepts, methods, and applications of selection experiments. University of California Press, Berkeley.

Swallow, J. G., P. Koteja, P. A. Carter, and T. Garland, Jr. 1999. Artificial selection for increased wheel-running activity in house mice results in decreased body mass at maturity. J. Exp. Biol. 202:2513–2520.

Tavares, W. C., and L. M. Pessôa. 2020. Effects of size, phylogeny and locomotor habits on the pelvic and femoral morphology of South American spiny rats (Rodentia: Echimyidae). Biol. J. Linn. Soc. 131:835–869.

Thompson, Z., I. A. T. Fonseca, W. Acosta, L. Idarraga, and T. Garland, Jr. 2024. Effects of food restriction on voluntary wheel-running behavior and body mass in selectively bred High Runner lines of mice. Physiol. Behav. 282:1114582.

Toro, E., A. Herrel, and D. Irschick. 2004. The evolution of jumping performance in caribbean *Anolis* lizards: solutions to biomechanical trade-offs. Am. Nat. 163:844–856.

Uesugi, Y., O. Taguchi, T. Noumura, and T. Iguchi. 1992. Effects of sex steroids on the development of sexual dimorphism in mouse innominate bone. Anat. Rec. 234:541–548.

Wainwright, P. C. 2005. Many-to-One Mapping of Form to Function: A General Principle in Organismal Design? Integr. Comp. Biol. 45:256–262.

Wallace, I. J., and T. Garland, Jr. 2016. Mobility as an emergent property of biological organization: insights from experimental evolution. Evol. Anthropol. 25:98–104.

Webb, E., J. Hennekam, N. E. Schwartz, T. Garland, Jr., and K. Jones. 2026. Modular adaptation of the ribcage in response to artificial selection for endurance running. Anat. Rec. In press.

Zelditch, M. L., and D. L. Swiderski. 2024. Correction: effects of procrustes superimposition and semilandmark sliding on modularity and integration: an investigation using simulations of biological data. Evol. Biol. 51:406–406.

Zelditch, M. L., D. L. Swiderski, and H. D. Sheets. 2026. Geometric morphometrics for biologists. Pp. i–iii *in* Geometric Morphometrics for Biologists. Elsevier.

Supplemental Files

File S1. Protocols for using 3D Slicer.

Supplementary_Material_Protocol 3dslicer_V10ProQuest.docx

File S2. R Code Markdown and Complete Results.

PelvisShape_Analysis_Code_40_Supp.docx